Spectroscopy of SU(4) gauge theory with two flavors of sextet fermions

Thomas DeGrand, Yuzhi Liu, Ethan T. Neil, Yigal Shamir, and Benjamin Svetitsky

Phys. Rev. D **91**, 114502 — Published 10 June 2015

DOI: 10.1103/PhysRevD.91.114502

COLO-HEP-586
YITP-15-4

Spectroscopy of SU(4) gauge theory with two flavors of sextet fermions

Thomas DeGrand,[1] Yuzhi Liu,[1] Ethan T. Neil,[1,2] Yigal Shamir,[3] and Benjamin Svetitsky[3,4]

[1]*Department of Physics, University of Colorado, Boulder, CO 80309, USA*
[2]*RIKEN-BNL Research Center, Brookhaven National Laboratory, Upton, NY 11973, USA*
[3]*Raymond and Beverly Sackler School of Physics and Astronomy, Tel Aviv University, 69978 Tel Aviv, Israel*
[4]*Yukawa Institute for Theoretical Physics, Kyoto University, Kyoto 606-8502, Japan*

We present a first look at the spectroscopy of SU(4) gauge theory coupled to two flavors of Dirac fermions in the two-index antisymmetric representation, which is a real representation. We compute meson and diquark masses, the pseudoscalar and vector meson decay constants, and the masses of six-quark baryons. We make comparisons with large-N_c expectations.

I. INTRODUCTION

Composite Higgs models [1–5] are frequently based on nonlinear sigma models. The most straightforward ultraviolet completion of such a model is a gauge theory with the corresponding spontaneous breaking of global symmetries. A symmetry-breaking scheme that is much discussed is $\mathrm{SU}(N) \to \mathrm{SO}(N)$. Such a breaking scheme can be accommodated in an $\mathrm{SU}(N_c)$ gauge theory where the fermions are in a real representation of the gauge group. Then $N = 2N_f$, where N_f is the number of flavors of Dirac fermions.

As the first stage in a program of investigating gauge theories of interest beyond the Standard Model, we here focus on the SU(4) gauge theory with fermions in the two-index antisymmetric representation (denoted AS2 henceforth). This is the sextet of SU(4), a real representation. We choose $N_f = 2$ flavors of Dirac fermions, so that the global chiral symmetry is also SU(4), which we expect to see spontaneously broken to SO(4).

This theory is a way station on the route to the SU(4) gauge theory with 5 Majorana fermions. That theory is the most economical way to realize the symmetry breaking of an SU(5)/SO(5) sigma model, which is the basis of, for instance, the Littlest Higgs model [6]. The SU(5)/SO(5) sigma model is also central to more recent composite-Higgs models [7–9]. Indeed, Vecchi [8] argued that the SU(4) theory with AS2 fermions is the most attractive candidate within this approach; Ferretti [9] elaborated on the phenomenology of this composite-Higgs model.[1] We can simulate the $N_f = 2$ theory with the standard Hybrid Monte Carlo (HMC) algorithm, while study of the theory with 5 Majorana fermions will require the more expensive rational HMC algorithm.

In this paper we present a study of the basic features of the $N_f = 2$ theory, namely, its phase diagram and spectrum; preliminary results were presented in [12]. The spectrum must exhibit multiplets of the unbroken SO(4) flavor symmetry. One feature of these multiplets is that mesons and diquarks transform into each other under SO(4). Because of this, baryons with more than two quarks are of particular interest; for reasons to be stated below, we study baryons made of six quarks.

We could simply present our results for spectroscopy without further analysis. However, we feel that, rather than just doing that, we should try to give them some context: we are studying a confining, chirally broken system. How are the masses and matrix elements we compute for our system different from, or similar to, what is seen in other confining and chirally broken systems?

The context we choose to use is the $1/N_c$ expansion. Theories with fermions in two-index representations have been studied extensively in a $1/N_c$ framework [13], as an alternative to the original $1/N_c$ expansion that deals with fermions in the fundamental representation [14, 15]. AS2 fermion loops are not suppressed at large-N_c, leading to different systematics than the conventional $1/N_c$ expansion.

Either $1/N_c$ expansion can in principle be applied to QCD, since for $N_c = 3$ the AS2 and fundamental representations are isomorphic. Furthermore, interesting equivalences to supersymmetric Yang–Mills theory in the $N_c \to \infty$ limit have been argued for theories with AS2 fermions [16–19], related to the orientifold equivalence among all gauge theories with two-index representations (adjoint, AS2, or symmetric) in the large-N_c limit [20–22]. This framework continues to attract interest.[2]

Our new data on the spectrum and decay constants for SU(3) and SU(4) theories with AS2 fermions will allow us to make a qualitative comparison to the scaling predictions of this alternative $1/N_c$ expansion. This comparison is made at a single value of the bare gauge coupling, in the confined and chirally broken phase of our lattice action. We have in hand already-published spectroscopy data for the SU(3), SU(5), and SU(7) gauge theories with fermions in the fundamental representation. These previous studies were performed in the quenched approximation, but a comparison to our new dynamical-fermion

[1] The models of Refs. [8, 9] include fermions in the fundamental representation in addition to the AS2, in order to give the top quark a mass via the partial-compositeness mechanism [10]. See also [11].

[2] See for example [23–29]. A recent review with emphasis on properties of baryons is given in [30].

data for the SU(3) theory, roughly matched in simulation volume and lattice spacing to the quenched data sets, shows little effect of quenching. This is because the dynamical fermion masses are not light enough to produce appreciable differences through loop effects. Of course, for study of the large-N_c limit with AS2 fermions, quenching is completely unjustified.

Baryons in large N_c are of long-standing interest in the traditional framework with fundamental-representation fermions. They can be analyzed as many-quark states [31] or can be taken to be topological objects in effective theories of mesons [32–35]. Large-N_c mass formulas for baryons have been presented in Refs. [23, 36–40]. An old review [41] summarizes much of this classic work.

Several recent lattice studies of baryon spectroscopy have touched on large-N_c considerations. The first [42] was a comparison of lattice Monte Carlo data for $N_c = 3$ baryons to large-N_c formulas. There are also three related studies at $N_c = 3$, 5, and 7, comparing quenched spectroscopy with $N_f = 2$ flavors of degenerate valence quarks [43]; spectroscopy with $N_f = 3$ flavors (two degenerate ones and a heavier strange quark) [44]; and $N_f = 2$ data to baryon chiral perturbation theory [45]. Finally, Ref. [46] reports calculations of quenched baryon spectroscopy in SU(4). The results of these studies all conform to large-N_c expectations for the fundamental representation; we will make comparisons of our spectrum to these results where appropriate.

We note in passing that the behavior of AS2 theories at finite baryon density has also attracted some theoretical interest [47, 48]. The SU(4) gauge theory is particularly useful for lattice work: Since the AS2 representation is real, the theory at finite baryon density presents no sign problem.

Now we proceed to the body of the paper. Section II collects some useful group-theoretic results about AS2 fermions in the SU(4) gauge theory, and their special symmetries. Six-quark baryons emerge as objects of interest. We present the lattice action and a new discretization issue in Sec. III. The choice of parameters used for spectroscopy was made after a scan of the bare parameter space (bare gauge coupling and hopping parameter). This scan revealed some of the phase structure of this system, which we present in Sec. IV. We describe our methods for obtaining spectra in Sec. V, and display tables of the resulting meson and baryon spectra. We then plot these results and offer comparisons among the SU(4) AS2 theory, the SU(3) theory, and quenched SU(3), SU(5), and SU(7) theories: for mesons in Sec. VI and for baryons in Sec. VII. Finally, Sec. VIII makes some phenomenological observations, summarizes our results, and suggests future directions.

II. GROUP THEORY AND SYMMETRIES

In this section we discuss the symmetry aspects of AS2 fermions in SU(4), specializing to $N_f = 2$. In Sec. II A we review some basic properties of real and pseudoreal representations, and how they are reflected in symmetries of the Wilson–Dirac operator and meson/diquark propagators.

In Sec. II B we turn to global symmetries. The pattern of chiral symmetry breaking in SU(4) AS2 is different from that in SU(3) gauge theories with fundamental-representation fermions, because the AS2 fermions live in a real representation of the gauge group. The usual breaking pattern, $\mathrm{SU}(N_f) \times \mathrm{SU}(N_f) \to \mathrm{SU}(N_f)$, is replaced by $\mathrm{SU}(2N_f) \to \mathrm{SO}(2N_f)$ [49–51]. There are $2N_f^2 + N_f - 1$ Nambu–Goldstone bosons (NGBs), nine in all for $N_f = 2$. A consequence of reality is that, in addition to meson ($q\bar{q}$) and baryon states, there are also diquark states. Symmetries associated with the fermions' reality means that all diquark correlators are identical to corresponding meson ones. For example, the diquarks are needed to fill out the NGB multiplets. The nine NGBs consist of three isotriplets: one multiplet is $q\bar{q}$, one is qq and one is $\bar{q}\bar{q}$.

The global symmetry of the $N_f = 2$ AS2 theory is thus $\mathrm{SU}(2N_f) = \mathrm{SU}(4)$. After dynamical symmetry breaking, the unbroken symmetry is SO(4). We elaborate on this symmetry breaking pattern, focusing on how the two invariant SU(2) subgroups of SO(4) are realized. As an example, we classify the 9 Nambu–Goldstone bosons under the unbroken symmetry. In Sec. II C we recall the equivalence between the AS2 representation of color SU(4) and the vector representation of SO(6). We use this equivalence to introduce the color-singlet state of 6 AS2 fermions, which is fully antisymmetric in its color indices. The remainder of the section explains why the six-quark baryons are the interesting baryonic states, and describes how we construct baryon operators.

A. Symmetries of real and pseudoreal representations

We begin by recalling how basis states of the AS2 irreducible representation are built from color basis states $|i\rangle$ in the fundamental representation. The basis states of the antisymmetric representation are

$$|ij\rangle = \frac{1}{\sqrt{2}} \Big(|i\rangle\,|j\rangle - |j\rangle\,|i\rangle \Big), \qquad 1 \le i < j \le N_c\,. \quad (2.1)$$

There are $N_c(N_c-1)/2$ basis states—six states for $N_c = 4$. Starting from the transformation rule $|i\rangle' = \sum_k U_{ik}\,|k\rangle$, the AS2 states transform as

$$\begin{aligned} |ij\rangle' &= \frac{1}{\sqrt{2}} \Big(|i\rangle'\,|j\rangle' - |j\rangle'\,|i\rangle' \Big) \\ &= \sum_{k<l} \Big(U_{ik}U_{jl} - U_{jk}U_{il} \Big)\,|kl\rangle \\ &\equiv \sum_{k<l} U_{[ij][kl]}\,|kl\rangle\ . \end{aligned} \quad (2.2)$$

Equation (2.2) provides the composition rule for $U_{[ij][kl]}$, the link matrices in the AS2 representation, in terms of links U_{ik} which are elements of the fundamental representation of SU(N_c).

The AS2 representation of SU(4) is real. Correlators of fermionic bilinears reflect this reality. This is similar to the situation in $N_c = 2$ where the fundamental representation is pseudoreal. As in the case of the two-color theory with fundamental fermions, which was nicely described in Ref. [52], for any (pseudo)real representation there is an exact identity between a meson correlator and a corresponding diquark correlator,

$$\begin{aligned}&\left\langle \bar{u}(x)\Gamma d(x)\, \bar{d}(y)\Gamma^\dagger u(y)\right\rangle \\ &\quad = \left\langle \bar{u}(x)\Gamma \left(SC\bar{d}(x)^T\right)\, \left(d(y)^T SC\right)\Gamma^\dagger u(y)\right\rangle \ , \end{aligned} \tag{2.3}$$

where $u(x)$ and $d(x)$ are the two flavors of Dirac fermions and Γ is a Dirac matrix. Let us see how this comes about.

The matrix S is defined as follows. A real or pseudoreal irreducible representation is self-conjugate, meaning that there is a quadratic form S such that for two vectors a and b the product $a^T S b$ is a singlet. Demanding invariance under $a = Ua'$, $b = Ub'$, we find

$$U^T S U = S, \tag{2.4}$$

which implies that the Hermitian generators T_a satisfy

$$T_a^T S = T_a^* S = -S T_a. \tag{2.5}$$

The entries of S are real, $S^* = S$, and it satisfies $S^{-1} = S^T$. For a real representation $S \equiv R = R^T$ is symmetric, whereas for a pseudoreal representation $S \equiv P = -P^T$ is antisymmetric. For the AS2 representation of SU(4), it is realized as

$$S\psi_{[ij]} = \sum_{k<l} \epsilon_{ijkl}\psi_{[kl]}. \tag{2.6}$$

(Note that $\epsilon_{ijkl} = \epsilon_{klij}$, so S is symmetric as it should be for a real representation.)

The matrix C occurring in Eq. (2.3) is the usual charge-conjugation matrix, which satisfies $C\gamma_\mu = -\gamma_\mu^T C$, and $C^{-1} = C^\dagger = C^T = -C$. We recall that charge-conjugation symmetry acts as[3]

$$\begin{aligned} \psi &\to C\,\bar{\psi}^T \ , && && (2.7a)\\ \bar{\psi} &\to \psi^T C \ , && && (2.7b)\\ A_\mu &\to -A_\mu^* && \text{(continuum)} \ , && (2.7c)\\ U_\mu &\to U_\mu^* && \text{(lattice)} \ . && (2.7d) \end{aligned}$$

We are now ready to derive the identity (2.3). Consider any fermion action that is invariant under the charge-conjugation symmetry (2.7) when the fermions belong to a complex representation. If we now take the fermions to be in a real representation ($S \equiv R$), then the fermion action will be invariant under the following discrete symmetry:

$$\begin{aligned} \psi &\to RC\,\bar{\psi}^T \ , && && (2.8a)\\ \bar{\psi} &\to \psi^T C R \ , && && (2.8b)\\ A_\mu &\to A_\mu && \text{(continuum)} \ , && (2.8c)\\ U_\mu &\to U_\mu && \text{(lattice)} \ . && (2.8d) \end{aligned}$$

Thanks to the reality condition (2.4), the inclusion of R in the fermions' transformation rule makes up for the fact that the gauge field does not transform. For a pseudoreal representation ($S \equiv P$), the discrete symmetry is

$$\begin{aligned} \psi &\to PC\,\bar{\psi}^T \ , && (2.9a)\\ \bar{\psi} &\to -\psi^T C P \ . && (2.9b) \end{aligned}$$

We may apply the transformation (2.8) [or (2.9)] to a single Dirac fermion. This is unlike the usual charge conjugation (2.7), which acts on the gauge field as well and must be applied to all fields simultaneously. For both real and pseudoreal representations, it follows that the (lattice) Dirac operator satisfies the identity

$$SCD^T S^{-1} C^{-1} = -SCD^T S^{-1} C = D, \tag{2.10}$$

and Eq. (2.3) follows.

We comment in passing that for Wilson fermions, $\gamma_5 D^\dagger \gamma_5 = D$. Together with (the Hermitian conjugate of) Eq. (2.10) this implies

$$S\gamma_5 C D^* S \gamma_5 C = -D \ , \tag{2.11}$$

and hence that the fermion determinant is real.

B. The unbroken SO(4) symmetry and baryon number

In a gauge theory with N_f Dirac fermions in a real representation, the global symmetry is SU($2N_f$). After chiral symmetry breaking, the unbroken symmetry is SO($2N_f$). These statements are most obvious when the theory is formulated in terms of Majorana fermions. Invariance under the transformation (2.8) allows each Dirac field to be broken up into two Majorana fields, with no mixing in the action as long as there are no mass terms. The number of independent Majorana (or Weyl) fields is $N_{\rm Maj} = 2N_f$, making the global symmetry SU($2N_f$). The fermion condensate is a Majorana-fermion bilinear which, for a real representation, is symmetric in its color indices. As the expectation value of a scalar operator, it is antisymmetric in its spin indices, and so it must be symmetric in its (Majorana) flavor indices. It then follows that the unbroken symmetry is SO($2N_f$) [49–51].

Since we elect to work with two AS2 Dirac fermions (instead of four Majorana fermions), we should understand how the SO(4) unbroken symmetry is realized on

[3] The Euclidean rules (2.7a) and (2.7b) are consistent with the Minkowskian relation $\bar{\psi} = \psi^\dagger\gamma_0$, where we have identified $\gamma_0 \equiv \gamma_4$.

them. SO(4) is doubly covered by SU(2) × SU(2). We will now work out how the two SU(2) groups act on our Dirac fermions. As we will see, one of the SU(2) groups may be identified with isospin, while the baryon number symmetry becomes a subgroup of the other SU(2).

We start with the observation that SO(4) is the symmetry group of the three-sphere S^3, which in turn can be identified with the SU(2) group manifold via $\hat{x} = x_4 + i\sum_{a=1}^{3} x_a\sigma_a$, where σ_a are the Pauli matrices and $\sum_{\mu=1}^{4} x_\mu^2 = 1$. The product group SU(2) × SU(2) is then realized as[4]

$$\hat{x} \to g\hat{x}h^\dagger \ , \qquad g, h \in \mathrm{SU}(2) \ . \tag{2.12}$$

In order to keep track of the SU(2) transformation properties it is convenient to rearrange the four real coordinates into two complex ones. We choose $\phi_1 = x_4 + ix_3$, $\phi_2 = -x_2 + ix_1$, so that

$$\hat{x} = \begin{pmatrix} \phi_1 & -\phi_2^* \\ \phi_2 & \phi_1^* \end{pmatrix} \ , \qquad -\hat{x}^\dagger = \begin{pmatrix} -\phi_1^* & -\phi_2^* \\ \phi_2 & -\phi_1 \end{pmatrix} \ . \tag{2.13}$$

(The minus sign in front of $\hat{x}^\dagger$ is introduced for convenience below.)

The transformation properties under left-multiplication are now obvious. The left column of the $\hat{x}$ matrix is an SU(2) doublet (ϕ_1, ϕ_2). Denoting this doublet as Φ_α, the right column is $\Phi'_\alpha = \epsilon_{\alpha\beta}\Phi^*_\beta$, which again transforms in the fundamental representation of SU(2).

Next, in order to obtain the behavior under right-multiplication we consider the left-action of h on $-\hat{x}^\dagger$. We read off the right-multiplication doublets: $(-\phi_1^*, \phi_2)$ from the left column of $-\hat{x}^\dagger$, and $(-\phi_2^*, -\phi_1)$ from its right column. The left- and right- doublets are related by interchanging ϕ_1 with $-\phi_1^*$.

We now turn to our AS2 theory. The role of real coordinates is played by Majorana fermions, whereas that of complex coordinates is played by Dirac fermions. What takes the place of complex conjugation is the transformation (2.8). We may arrange our two Dirac fermions, u and d, as well as their anti-fermions, in complete analogy with Eq. (2.13),

$$\Psi = \begin{pmatrix} u & -RC\bar{d}^T \\ d & RC\bar{u}^T \end{pmatrix} \ . \tag{2.14}$$

Motivated by this arrangement we will refer to the left-multiplication SU(2) as isospin symmetry, and to the right-multiplication SU(2) as custodial symmetry. It goes without saying that the two SU(2)'s play a similar role, and the only "preference" for the left-multiplication doublets is in our notation. The isospin and custodial symmetries get interchanged by $u \leftrightarrow -RC\bar{u}^T$, which is basically the discrete symmetry (2.8) applied to the u quark only.[5]

Let us take a closer look at the custodial-symmetry generator σ_3. With reference to Eq. (2.13), its action on the second row of $\hat{x}$, which is the multiplet (ϕ_2, ϕ_1^*), is $\delta\phi_2 = \phi_2$ and $\delta\phi_1^* = -\phi_1^*$, or $\delta\phi_1 = \phi_1$. Thus ϕ_1 and ϕ_2 transform with the same phase. A translation to the language of Eq. (2.14) is that the custodial σ_3 is just the baryon number. In a two-flavor theory of complex-representation fermions, the unbroken symmetries are isospin and the U(1) of baryon number. In our case, the U(1) is enlarged to a second SU(2) that we call the custodial symmetry, whose two other generators thus raise or lower the baryon number.

Now that we have understood the unbroken symmetry structure, let us consider a few simple applications. As a first exercise, one can show that the transformation (2.8), when applied to the u and d fields simultaneously, is in fact an element of SO(4). Indeed, consider $\Psi \to -i\sigma_2\Psi\, i\sigma_2$, which is a simultaneous rotation in isospin and custodial SU(2). This is just $u \to RC\bar{u}^T$, and the same for d.

We next turn to the NGBs. Start with the familiar triplet of pions: $\bar{d}\gamma_5 u$, $\bar{u}\gamma_5 d$, and $\bar{u}\gamma_5 u - \bar{d}\gamma_5 d$. Now let us apply a custodial rotation of the form $\exp(i\theta\sigma_1)$. Then $\bar{u}\gamma_5 d$ rotates into a linear combination of itself, of $d^T RC\gamma_5 d$, and of $\bar{u}\gamma_5 RC\bar{u}^T$. The last two are respectively a diquark and an anti-diquark, each belonging to an isospin-1 multiplet. It follows that there are indeed 9 NGBs, which fall into 3 isospin triplets: one made of diquarks, one of anti-diquarks, and one of quark-antiquark pairs.

C. SU(4) ↔ SO(6) correspondence and the six-quark baryon

In this subsection we first work out in detail the identification between the AS2 representation of SU(4) and the vector representation of SO(6). This allows us to construct a fully antisymmetric color wave function for six AS2 fermions, which will be common to all our baryon states.

In Sec. II A we labeled the components of the AS2 representation by an index pair. We can alternatively introduce a single index $a = 1, \ldots, 6$, with the correspondence $\psi_1 = \psi_{[12]}$, $\psi_2 = \psi_{[13]}$, …, $\psi_6 = \psi_{[34]}$. In the ψ_a basis

[4] The product-group elements $g = -1$, $h = 1$, and $g = 1$, $h = -1$, coincide when they act on $\hat{x}$. Hence SU(2) × SU(2) is a double covering of SO(4).

[5] We are free to add minus signs on the right-hand sides of Eqs. (2.8a) and (2.8b) simultaneously.

the matrix R of Sec. II A takes the explicit form

$$R = \begin{pmatrix} 0 & 0 & 0 & 0 & 0 & 1 \\ 0 & 0 & 0 & 0 & -1 & 0 \\ 0 & 0 & 0 & 1 & 0 & 0 \\ 0 & 0 & 1 & 0 & 0 & 0 \\ 0 & -1 & 0 & 0 & 0 & 0 \\ 1 & 0 & 0 & 0 & 0 & 0 \end{pmatrix} . \tag{2.15}$$

The inner product of two AS2 spinors,

$$\sum_{i<j} \sum_{k<l} \epsilon_{ijkl} \psi_{[ij]} \chi_{[kl]} = \psi_a R_{ab} \chi_b = \psi^T R \chi \ , \tag{2.16}$$

is SU(4)-invariant by virtue of Eq. (2.4).

We can recover the standard formulation of SO(6) by applying a U(6) basis transformation to the AS2 states. As a first step, we permute the basis elements and multiply one of them by a minus sign, bringing R to the block diagonal form

$$R = \begin{pmatrix} \sigma_1 & 0 & 0 \\ 0 & \sigma_1 & 0 \\ 0 & 0 & \sigma_1 \end{pmatrix} . \tag{2.17}$$

For a further change of basis, we note that

$$\sigma_1 = \tau^2, \text{ with } \tau = \begin{pmatrix} z & z^* \\ z^* & z \end{pmatrix} , \tag{2.18}$$

where $z = (1+i)/2$. We denote by Q the 6×6 matrix with three blocks of the matrix τ along the main diagonal. Upon performing the basis change

$$\psi \to \psi' = Q\psi \ , \tag{2.19}$$

the inner product becomes[6]

$$\psi^T R \chi \to \psi^T Q^T R Q \chi = \psi^T \chi \ . \tag{2.20}$$

The inner product has now taken its standard SO(6) form. Under the same basis change, the AS2 SU(4) generators transform as

$$T_a \to Q T_a Q^\dagger \ . \tag{2.21}$$

Using the properties of the R and Q matrices and Eq. (2.5) it follows that

$$(Q T_a Q^\dagger)^T = Q^\dagger T_a^T Q = Q R T_a^T R Q^\dagger = -Q T_a Q^\dagger \ . \tag{2.22}$$

In the new basis, the generators are antisymmetric (and purely imaginary), as required for the standard basis of SO(6).

As an application of the above, we can show that the fully antisymmetric six-quark wave function

$$B = \epsilon_{a_1 a_2 \cdots a_6} \psi_{a_1} \psi_{a_2} \cdots \psi_{a_6} \ , \tag{2.23}$$

is gauge invariant (we suppress flavor indices). To prove this, start from

$$B' = \epsilon_{a_1 a_2 \cdots a_6} \psi'_{a_1} \psi'_{a_2} \cdots \psi'_{a_6} \ , \tag{2.24}$$

where the ψ' basis was introduced in Eq. (2.19). This operator is clearly gauge invariant, because in the ψ' basis the SU(4) elements are mapped to orthogonal SO(6) matrices, and the epsilon tensor in Eq. (2.24) is the invariant 6-dimensional tensor. Going back to the original basis we have

$$B' = \epsilon_{a_1 a_2 \cdots a_6} (Q\psi)_{a_1} (Q\psi)_{a_2} \cdots (Q\psi)_{a_6} \ . \tag{2.25}$$

The matrix Q is unitary, and so it leaves invariant the epsilon tensor, up to a factor of $\det Q = -i$. It follows that $B' = iB$, and hence B is gauge invariant as well. We use the fully antisymmetric color wave function (2.23) in the construction of all baryon operators.

D. Diquarks, tetraquarks, and baryons

In constructing states with baryon number, we note first that a color singlet state has to be made of an even number of quarks. Thus we begin with diquarks. As we have seen, the real color representation of the quarks leads to the conclusion that diquarks are degenerate with mesons. Their color wave function involves the inner product (2.16)

$$D = \psi_a^f R_{ab} \psi_b^g, \tag{2.26}$$

where f, g stand for the spin and flavor indices. Because R is symmetric, diquarks have a symmetric color wave function. Viewed through the prism of the nonrelativistic quark model, which puts the two quarks in an s-wave, the product of their spin and isospin wave functions must then be antisymmetric.[7] For (pseudo)scalars, the spin wave function is antisymmetric, and the isospin wave function should be symmetric. Those that are NGBs have $I = 1$, as seen above. States with higher angular momentum are, of course, also possible. These would include the diquark analogs of (axial) vector and tensor mesons.

The only way to construct a color-singlet *tetraquark* state is by pairwise contraction of the color indices,

$$T = (\psi_a^f R_{ab} \psi_b^g)(\psi_c^h R_{cd} \psi_d^i). \tag{2.27}$$

One can permute the spin-flavor indices to derive a total of three pairwise coupling schemes. Linear combinations of these schemes will have mixed symmetry under color, but each term will still factor into two color-singlet diquarks. Moreover, by applying an RC transformation to

[6] The inner product is invariant under SU(4) [equivalently SO(6)] transformations, not under general U(6) transformations.

[7] Since we are talking about diquarks rather than mesons, both quarks are in the $\sigma_3 = +1$ state of the custodial SU(2).

one quark flavor at a time, one finds that the tetraquarks are degenerate with $\bar{\psi}\psi\psi\psi$ and $\bar{\psi}\bar{\psi}\psi\psi$ states. It is an open question as to whether the tetraquark states in this theory will be meson and diquark scattering states, or bound states; we will not study them further here.

The first baryonic state that cannot be factored into smaller color-singlet components is the six-quark baryon written in Eq. (2.23). It differs essentially from the various pairwise contractions in that it is fully antisymmetric in color. This makes it similar to the baryon of QCD, and indeed similar to baryons made of fundamental-representation quarks for any N_c. Bolognesi [24] has argued that this is the correct baryonic state for studying the large-N_c limit of gauge theories with AS2 quarks. In general, he finds that baryons made of $N_b = N_c(N_c-1)/2$ constituents in the AS2 color representation fit well into a Skyrmion picture. While our construction of the wave function (2.23) relies on special properties of the $N_c = 4$ theory, Bolognesi has given an existence proof for a fully antisymmetric, gauge invariant color wave function for any N_c.

E. Interpolating fields

A lattice simulation needs interpolating fields with an appropriate set of quantum numbers. As noted above, since it is fully antisymmetric under exchange, the AS2 color wave function (2.23) is similar to the color wave function of baryons made of fundamental representation fermions. The multiplet patterns are therefore similar as well. The construction of baryon correlators was discussed in detail in a previous work by one of us [43]. Here we give a brief synopsis.

A convenient set of interpolating fields for baryons are operators which create nonrelativistic quark model trial states. They are diagonal in a γ_0 basis. In the case at hand, a generic two-flavor baryon interpolating field made out of k up quarks and $6-k$ down quarks can be written as

$$O_B = \epsilon_{a_1\cdots a_6}\, C^{s_1\cdots s_6}\, u^{s_1}_{a_1}\cdots u^{s_k}_{a_k}\, d^{s_{k+1}}_{a_{k+1}}\cdots d^{s_6}_{a_6}\ , \qquad (2.28)$$

where summation over all color and spin indices is implied. (We are free to put all the u's to the left of all the d's.) The C's are an appropriate set of Clebsch–Gordan coefficients. The spin wave function of each quark type, u or d, must be totally symmetric.

Next we may take linear combinations of the O_B's to construct operators with definite isospin quantum numbers. For states built of two flavors of quarks all in the same spatial wave function, multiplets are locked in equal values for angular momentum J and isospin I. Thus we have states with $I = J = 3$, 2, 1, and 0.

The two-baryon correlator must include all nonzero contractions of creation operators at the source and annihilation operators at the sink. For each flavor, this gives a determinant of quark propagators. These must be summed over all the ways that colors can be apportioned between the quarks. For the analog of the Δ^{++}, the state with $I = I_3 = J = J_3 = N_b/2 = 3$, this is a single term. The number of terms increases rapidly as the angular momentum decreases, raising the computational cost of the calculation. (This was an issue for the $N_c = 7$ baryons of Ref. [43].) Fortunately, $N_b = 6$ is not too large and the calculation always remains manageable.

With baryon number as its third generator, our baryons are highest-weight states of the custodial symmetry. In this paper, we are content with studying these states, and we do not consider the six-quark states with smaller baryon number that would be needed to fill in multiplets of the custodial symmetry.

III. LATTICE ACTION

We define the lattice theory with the usual Wilson plaquette gauge action and with Wilson–clover fermions. The fermion action uses gauge connections defined as normalized hypercubic (nHYP) smeared links [53–55]. The gauge coupling is set by the parameter $\beta = 2N_c/g_0^2$. We take the two Dirac flavors to be degenerate, with common bare quark mass introduced via the hopping parameter $\kappa = (2m_0^q a + 8)^{-1}$. As is appropriate for nHYP smearing [56], we fix the clover coefficient at its tree level value, $c_{\rm SW} = 1$.

nHYP smearing introduces a new type of discretization error, peculiar to the real representation of the matter field. Our prescription for smearing the fermion's gauge connection begins with applying the nHYP formulas [55] to the fundamental gauge link, and then the resulting fat link V_{ik} is promoted to the AS2 representation via Eq. (2.2). The problem is that V_{ik} is in fact an element of $\mathrm{U}(N_c)$, not $\mathrm{SU}(N_c)$, viz.,

$$V_{ik} = e^{i\theta} U_{ik}, \qquad (3.1)$$

where both the SU(4) part U_{ik} and the U(1) phase θ are determined by our smearing recipe. Having its origin in the smearing formulas, this U(1) phase is a discretization effect, and hence it must vanish like some power of the lattice spacing in the continuum limit. When we apply Eq. (2.2) to construct the AS2 fat link $V_{[ij][kl]}$ from the original fat link V_{ik}, we end up with $V_{[ij][kl]} = e^{2i\theta} U_{[ij][kl]}$. Because of this unphysical phase, the AS2 fat link $V_{[ij][kl]}$ fails to satisfy the reality condition (2.4). This in turn leads to violation of relations like Eq. (2.3).

We can gauge the severity of this discretization error by looking at violations of Eq. (2.3). Comparing meson and diquark propagators calculated on single configurations, we have found differences in the third significant digit. Similar effects are seen in the eigenvalue spectrum of the Wilson–clover operator. To the extent that this error creeps into the generation of configurations, there is no cause for concern.

Nonetheless, the breaking of the symmetry (2.4) in the observables is annoying. A way to fix this problem is to

replace the AS2 fat link $V_{[ij][kl]}$ obtained from Eq. (2.2) with

$$V'_{[ij][kl]} = \frac{1}{2}(V + SV^*S)_{[ij][kl]} \tag{3.2}$$

before calculating observables. (This can be regarded as a partial quenching, since the correction here is applied only to the valence fermions; one may use V' for the sea fermions as well, but since we had already generated ensembles without this correction we chose not to do so.)

The new AS2 link $V'_{[ij][kl]}$ satisfies Eq. (2.4) by construction, at the price of being slightly non-unitary. We compared spectroscopy with and without this correction for a $12^3 \times 24$ data set at one of our parameter values ($\beta = 9.6$, $\kappa = 0.1285$). The differences turned out to lie well under one standard deviation. We conclude that the discretization error and the partial quenching (3.2) are benign.

Wilson fermions break chiral symmetry explicitly. In the familiar case of a complex representation, the symmetry breaking pattern of the two-flavor continuum theory is $\mathrm{SU}(2)_L \times \mathrm{SU}(2)_R \to \mathrm{SU}(2)_V$. With Wilson fermions, the breaking of $\mathrm{SU}(2)_L \times \mathrm{SU}(2)_R$ becomes explicit, and only $\mathrm{SU}(2)_V$ (and, of course, baryon number) is a good symmetry. While the NGBs become massless when we tune κ to its critical value κ_c, full chiral symmetry is only restored in the continuum limit. For $\kappa > \kappa_c$ one enters the Aoki phase [57, 58], where one of the NGB fields condenses, and $\mathrm{SU}(2)_V$ is broken spontaneously.

In our model, the spontaneous symmetry breaking $\mathrm{SU}(4) \to \mathrm{SO}(4)$ of a real representation turns into explicit breaking with Wilson fermions. Only SO(4) is a good symmetry on the lattice, and the full SU(4) flavor symmetry is only recovered in the continuum limit. For $\kappa < \kappa_c$ the NGBs discussed in Sec. II—mesons and diquarks—acquire a mass. For $\kappa > \kappa_c$ again one expects to find an Aoki phase. The case of 5 AS2 Majorana fermions (relevant for the SU(5)/SO(5) non-linear sigma model mentioned in the introduction) was recently studied using chiral Lagrangian techniques in Ref. [59].

IV. PHASE DIAGRAM

As preparation for spectroscopy, we have to find couplings in the confining and chirally broken phase. The phase diagram of Wilson fermion actions in the (β, κ) plane can be complicated, depending on the fermion content and the specific action used [57–61]. Figure 1 shows the phase diagram we have observed for the SU(4) AS2 action considered in this paper. The curves shown indicate:

1. $\kappa_c(\beta)$, the critical value of the hopping parameter where the quark mass m_q vanishes.

2. $\kappa_t(\beta)$, the curve of the thermal phase transition. Its location shifts with the lattice size, and two lattice sizes are indicated.

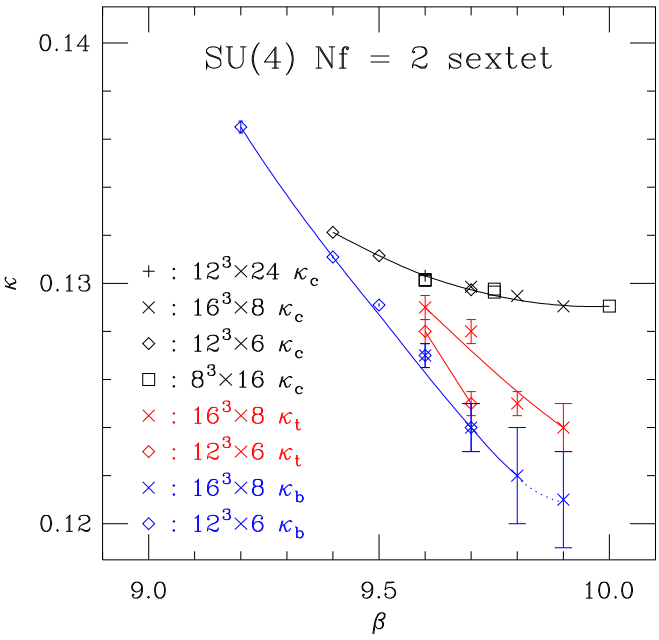

FIG. 1: Phase diagram of the SU(4) AS2 theory in the (β, κ) plane. The solid lines are drawn to guide the eye and are not a fit to the data. From right to left: κ_c, $\kappa_t(N_t = 8)$, $\kappa_t(N_t = 6)$, and κ_b. The dotted line indicates weakening of the bulk transition to a crossover.

3. $\kappa_b(\beta)$, the curve of a bulk phase transition that does not move with lattice size.

We discuss each in turn.

A. κ_c determination

We define the quark mass through the axial Ward identity (AWI), which relates the divergence of the axial current $A^a_\mu = \bar\psi\gamma_\mu\gamma_5(\tau^a/2)\psi$ to the pseudoscalar density $P^a = \bar\psi\gamma_5(\tau^a/2)\psi$. At zero three-momentum we have

$$\partial_t \sum_{\mathbf{x}} \langle A^a_0(\mathbf{x}, t)\mathcal{O}^a\rangle = 2m_q \sum_{\mathbf{x}} \langle P^a(\mathbf{x}, t)\mathcal{O}^a\rangle\,. \tag{4.1}$$

where $\mathcal{O}^a$ is a source, here taken to be a smeared "Gaussian shell" source. The critical $\kappa_c(\beta)$ line is determined through the vanishing of the quark mass m_q. As noted in Fig. 1, we use several lattice sizes $N_s^3 \times N_t$. When $N_t > N_s$, t labels the usual temporal direction, but when $N_t < N_s$, we choose one of the spatial directions to be t in Eq. (4.1) from correlators taken along one of the spacial directions of the lattice (so that the sum over x in Eq. 4.1 includes two directions with periodic fermion boundary conditions and one antiperiodic direction).

One example of the κ dependence of the quark mass m_q is shown in the left panel of Fig. 2. The zero-crossing at κ_c is apparent, as is a discontinuity in the $m_q(\kappa)$. The latter is a signal of a bulk transition, which we discuss

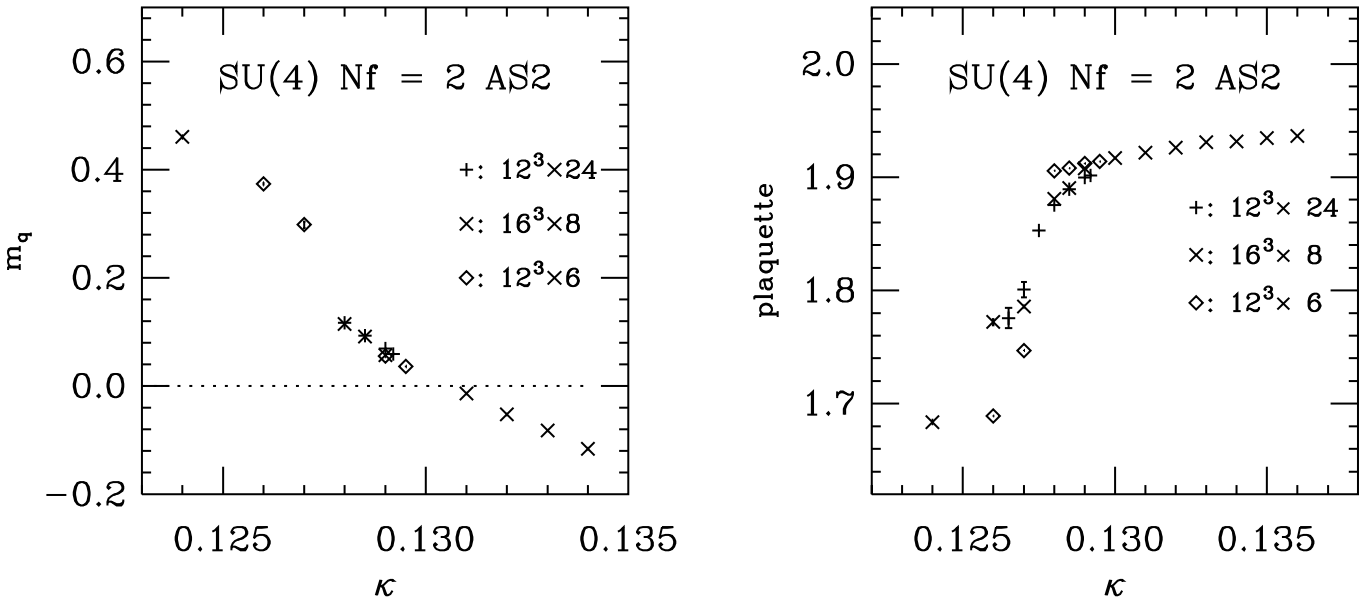

FIG. 2: Left: Quark mass m_q as a function of κ in different volumes at $\beta = 9.6$. Right: Average plaquette as a function of κ in different volumes at $\beta = 9.6$.

below in Sec. IV C. We note that there is little volume-dependence in $\kappa_c(\beta)$. We plot $\kappa_c(\beta)$ from all the volumes in Fig. 1 as a black line.

B. κ_t determination

The finite temperature transition lines $\kappa_t(\beta)$ are determined from the behavior of the Polyakov loop L. With AS2 fermions, the Z_4 center symmetry of the pure gauge theory symmetry is broken only to Z_2 and therefore there is a true confinement phase transition in our theory. $\langle L\rangle = 0$ in the low-temperature phase, while in the high-temperature phase $\langle L\rangle$ orders along the real axis. Typical scatter plots of the Polyakov loop in the two phases are shown in the left panel of Fig. 3. The average Polyakov loop as a function of κ at four different β values for a $16^3 \times 8$ volume are shown in the right panel of Fig. 3.

The $\kappa_t(\beta)$ lines for two different volumes, $16^3 \times 8$ and $12^3 \times 6$, are shown in Fig. 1 as red lines. The transition moves to weaker coupling as N_t increases, as expected from asymptotic freedom.

C. κ_b determination

In addition to the temperature-dependent deconfinement lines $\kappa_t(\beta)$, our system exhibits another transition line $\kappa_b(\beta)$. Its presence is signaled by discontinuities in several observables, notably the average plaquette and the quark mass m_q. We find that the position of the discontinuity is independent of volume. This is a bulk transition associated with the particular lattice action we use; most likely it has nothing to do with continuum physics. The mechanism that triggers the bulk transition is not clear to us. Similar behavior has been observed in other lattice actions, when the number of fermionic degrees of freedom is large [57, 58, 60, 61]. A similar bulk transition has been observed in studies of the SU(4) pure-gauge theory at $\beta \sim 10.2$ [63].

We have already seen, in the left panel of Fig. 2, a discontinuity in the quark mass m_q at $\kappa \approx 0.127$ as we scan at $\beta = 9.6$. The right panel of Fig. 2 shows the average plaquette values for $\beta = 9.6$ in three different volumes. All the plaquette data show a sudden jump at the same value of κ.

The transition weakens in the large-β/small-κ region and appears to show only a smooth crossover at $\beta \approx 10.0$. The $\kappa_b(\beta)$ line, determined on two different volumes, $16^3 \times 8$ and $12^3 \times 6$, is sketched in Fig. 1 in blue. Further work is needed to understand the origin of this peculiar bulk transition. For the current study, however, we only need to make sure that our simulation is on the weak-coupling (large-β) side of this transition so that it has a direct connection to continuum physics.

κ	configurations	r_1/a
0.128	146	2.50(1)
0.1285	140	2.78(2)
0.129	200	2.97(2)
0.1292	161	3.22(3)

TABLE I: Parameters of the SU(4) AS2 simulations. All are at coupling $\beta = 9.6$, in volume $16^3 \times 32$.

V. SPECTROSCOPY

A. SU(4) AS2

Referring to the phase diagram, Fig. 1, we chose to simulate the SU(4) AS2 theory at $\beta = 9.6$ for a range of hopping parameter values $0.127 < \kappa < 0.130$, between the bulk transition and κ_c. Our simulation volumes were all $16^3 \times 32$, and the resulting spectra show that our chosen κ values kept us in the confining phase, $\kappa < \kappa_t$. Gauge-field updates used the HMC algorithm with a multi-level Omelyan integrator, including one level of mass preconditioning for the fermions; integration parameters were adjusted to maintain acceptance rates on the order of 70-80%. Gauge configurations were saved to disk every 10 updates. The simulations are summarized in Table I.

The coupling $\beta = 9.6$ gives a lattice spacing that is neither too large nor too small. For comparison with other theories, we fix the lattice spacing using the shorter version [64] of the Sommer [65] parameter r_1, defined in terms of the force $F(r)$ between static quarks: $r^2F(r) = -1.0$ at $r = r_1$. The real-world value is $r_1 = 0.31$ fm [66], and thus Table I shows that our lattice spacings would correspond to a length scale of approximately 0.1 fm in QCD. For later comparison, we plot both Sommer parameters for our simulations in Fig. 4.

In addition to the simulations listed in Table I, we used the $\kappa = 0.129$ lattices as a set of configurations on which we computed partially quenched (PQ) spectroscopy with four values of the valence quark mass, $\kappa_V = 0.1295$, 0.130, 0.1305, 0.131. These data sets used the full complement of $\kappa = 0.129$ configurations. Of course, their lattice spacing is the same as that of the $\kappa = 0.129$ set.

The correlation functions whose analysis produced our spectroscopy used propagators constructed in Coulomb gauge, whose sources were Gaussians. We used $\vec{p} = 0$ point sinks. We collected sets for several different values of the width R_0 of the source. These correlation functions are not variational since the source and sink are different. We begin each fit with a distance-dependent effective mass $m_{\rm eff}(t)$, defined to be $m_{\rm eff}(t) = \log C(t)/C(t+1)$ consistent with open boundary conditions for the correlator $C(t)$. Because our sources and sinks are not identical, $m_{\rm eff}(t)$ can approach its asymptotic value from above or below. We mixed data with different values of R_0 to produce correlators with relatively flat $m_{\rm eff}(t)$, which we then used in a full analysis involving fits to a wide range

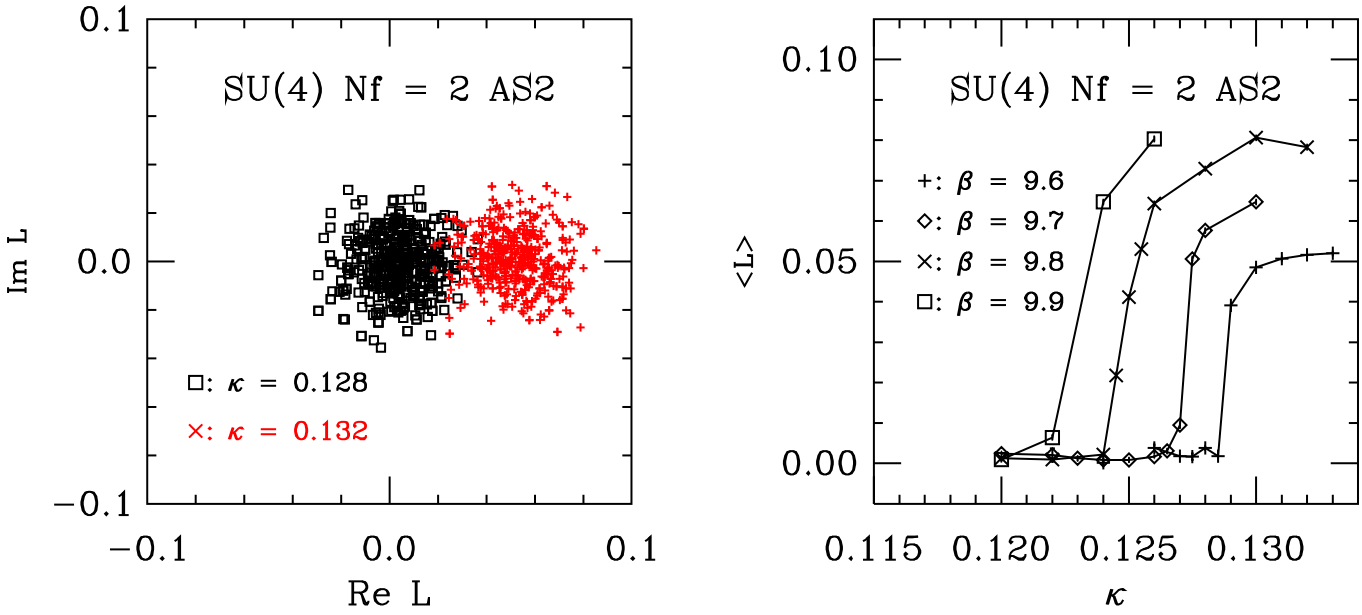

FIG. 3: Left: Scatter plots of the Polyakov loop in the two different phases on $16^3 \times 8$ lattices at $\beta = 9.6$. Right: Average Polyakov loop on $16^3 \times 8$ lattices for different β and κ values. The jump of the average Polyakov loop values for each β value signals a finite-temperature transition.

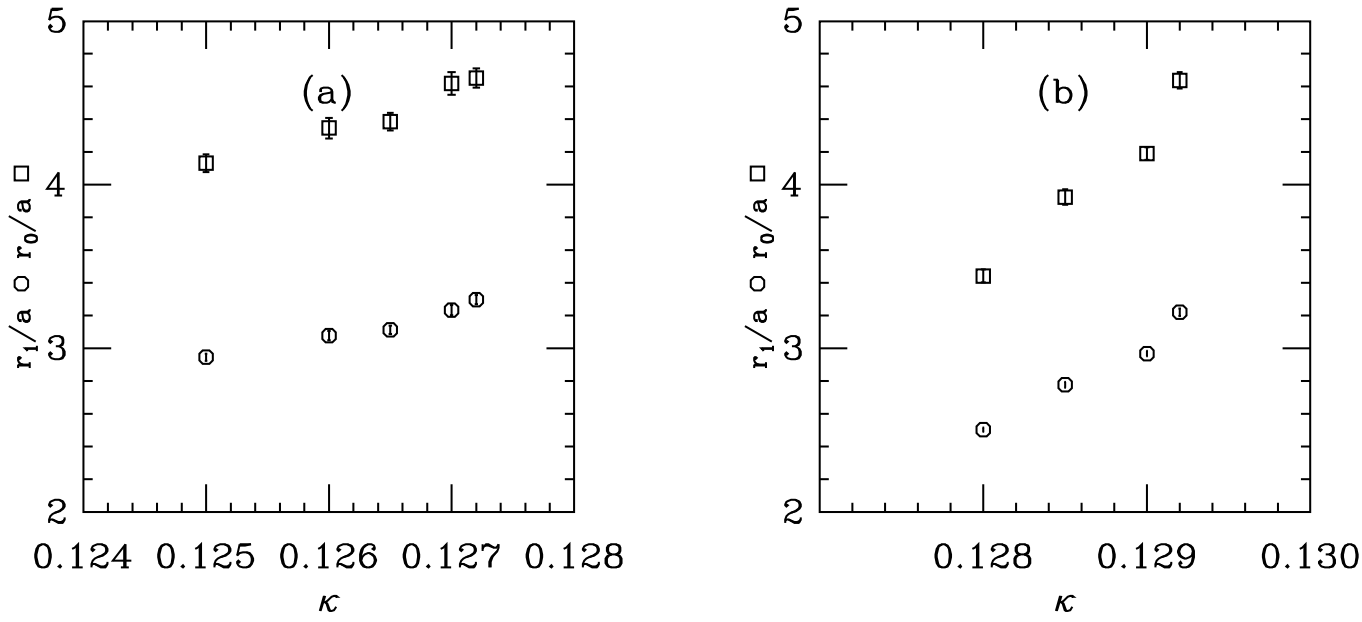

FIG. 4: Sommer parameters r_0 and r_1 from the dynamical SU(3) and SU(4) data sets [panels (a) and (b), respectively].

of t's. For more detail see Ref. [43].

Our resulting data are shown in Tables II, III, and IV. Table II shows the AWI mass and meson masses and decay constants. The pseudoscalar and vector meson decay constants, whose definitions are given in Eqs. (6.1) and (6.2) below, are given with lattice normalization for the fermion fields. The conversion to continuum numbers will be described below.

We also measured the masses of the $J = 0$ and $J = 1$ diquarks using nonrelativistic quark model interpolating fields, diquark analogs of the operators we used for baryons. Their masses are, as expected, degenerate with those of their mesonic partners.

Tables III and IV give the baryon masses and mass differences. These are computed together: a jackknife average of correlated, single-exponential fits to all four

κ	am_q	am_{PS}	am_V	af_{PS}	af_V
0.1280	0.124	0.680(1)	0.888(3)	0.978(10)	1.559(18)
0.1285	0.089	0.554(2)	0.749(6)	0.730(12)	1.563(29)
0.1290	0.067	0.462(1)	0.666(3)	0.693(5)	1.516(4)
0.1292	0.057	0.417(2)	0.602(2)	0.637(7)	1.501(7)
0.1295[a]	0.053	0.409(1)	0.630(2)	0.654(3)	1.570(8)
0.1300[a]	0.039	0.350(2)	0.596(3)	0.627(3)	1.627(11)
0.1305[a]	0.025	0.281(2)	0.561(4)	0.596(4)	1.699(13)
0.1310[a]	0.011	0.190(4)	0.529(8)	0.562(5)	1.783(18)

[a]Partially quenched: same gauge configurations as $\kappa = 0.129$.

TABLE II: AWI mass and meson spectra and decay constants from dynamical SU(4) AS2 simulations. f_{PS} and f_V have lattice normalization.

κ	$aM_B(3)$	$aM_B(2)$	$aM_B(1)$	$aM_B(0)$
0.1280	3.134(43)	3.055(32)	2.972(30)	2.923(32)
0.1285	2.608(35)	2.513(27)	2.442(25)	2.389(23)
0.1290	2.297(21)	2.212(17)	2.147(16)	2.113(16)
0.1292	2.046(24)	1.990(22)	1.948(22)	1.920(18)
0.1295[a]	2.179(26)	2.075(20)	2.002(20)	1.972(18)
0.1300[a]	2.094(37)	1.964(35)	1.902(29)	1.848(28)
0.1305[a]	1.984(77)	1.854(52)	1.826(95)	1.732(57)

[a]Partially quenched: same gauge configurations as $\kappa = 0.129$.

TABLE III: Baryon masses from dynamical SU(4) AS2 simulations. The number labels the angular momentum of the state: $M_B(3) = M_B(J = 3)$.

masses is performed and the differences are collected. This insures that the average mass difference is indeed the difference of the average masses. Since the data sets for the different angular-momentum states are identical, the uncertainty in the mass difference is usually smaller than the naive combination of uncertainties on the individual masses. These fits are over the range $5 \le t \le 10$. We have checked that fits over nearby t ranges are consistent within uncertainties with these results. We omit results for $\kappa_V = 0.131$ because the uncertainties in the baryon masses, especially the $J = 0$ baryon, are very large.

κ	$a\Delta M_{23}$	$a\Delta M_{13}$	$a\Delta M_{03}$
0.1280	0.079(29)	0.162(34)	0.210(34)
0.1285	0.095(26)	0.166(33)	0.219(34)
0.1290	0.086(16)	0.151(17)	0.185(19)
0.1292	0.056(16)	0.098(22)	0.126(12)
0.1295[a]	0.104(21)	0.177(22)	0.207(23)
0.1300[a]	0.131(36)	0.192(37)	0.247(37)
0.1305[a]	0.131(66)	0.159(117)	0.253(80)

[a]Partially quenched: same gauge configurations as $\kappa = 0.129$.

TABLE IV: Baryon mass splittings from dynamical SU(4) AS2 simulations. We define $\Delta M_{J_1 J_2} \equiv M_B(J_2) - M_B(J_1)$.

κ	configurations	r_1/a
0.125	100	2.95(2)
0.126	100	3.08(3)
0.1265	100	3.11(3)
0.127	100	3.23(3)
0.1272	100	3.30(3)

TABLE V: Parameters of the SU(3) simulations. All are at coupling $\beta = 5.4$, in volume $16^3 \times 32$.

κ	am_q	am_{PS}	am_V	af_{PS}	af_V
0.1250	0.105	0.559(2)	0.696(3)	0.456(6)	0.905(4)
0.1260	0.070	0.457(1)	0.619(3)	0.424(4)	0.993(8)
0.1265	0.059	0.402(3)	0.576(5)	0.385(3)	1.001(9)
0.1270	0.042	0.340(3)	0.531(5)	0.370(5)	1.050(9)
0.1272	0.028	0.307(3)	0.479(6)	0.318(7)	1.037(13)

TABLE VI: AWI mass and meson spectra and decay constants from dynamical SU(3) simulations. f_{PS} and f_V have lattice normalization.

B. SU(3) fundamental

We also generated a data set for SU(3) gauge fields coupled to $N_f = 2$ fermions in the fundamental representation. We did this for two (related) reasons. First, the SU(4) data sets include dynamical fermions, and so we felt that our comparison to $N_c = 3$ ought to be dynamical-to-dynamical. Second, all previous large-N_c comparisons were of quenched data sets. While quenching is not the state of the art, at the quark masses at which we work one might expect quenching artifacts to be small. A direct comparison seemed to be in order, and we found (as expected) that quenching effects indeed were small. This will be seen in the figures. Again, we used the clover action with nHYP links and $c_{SW} = 1$. The lattice volume was again $16^3 \times 32$ sites. We chose a gauge coupling $\beta = 5.4$. We saved configurations every five HMC trajectories. Parameter values are shown in Table V. Table VI shows mesonic observables from the dynamical SU(3) simulations, while Table VII shows baryon masses and mass differences. These numbers are taken from a jackknife average of the data sets with a fit range $5 \le t \le 10$.

VI. COMPARISONS: MESONS

We have presented our results for meson and baryon spectra and also for meson decay constants in the SU(4) AS2 and SU(3) theories in Sec. V. In this section and the next we will plot and rescale them for comparison with each other and with the quenched SU(N_c) theories, $N_c = 3$, 5, and 7. This is an important consistency check on our results, and discrepancies with predicted scaling may point to interesting directions for future study of

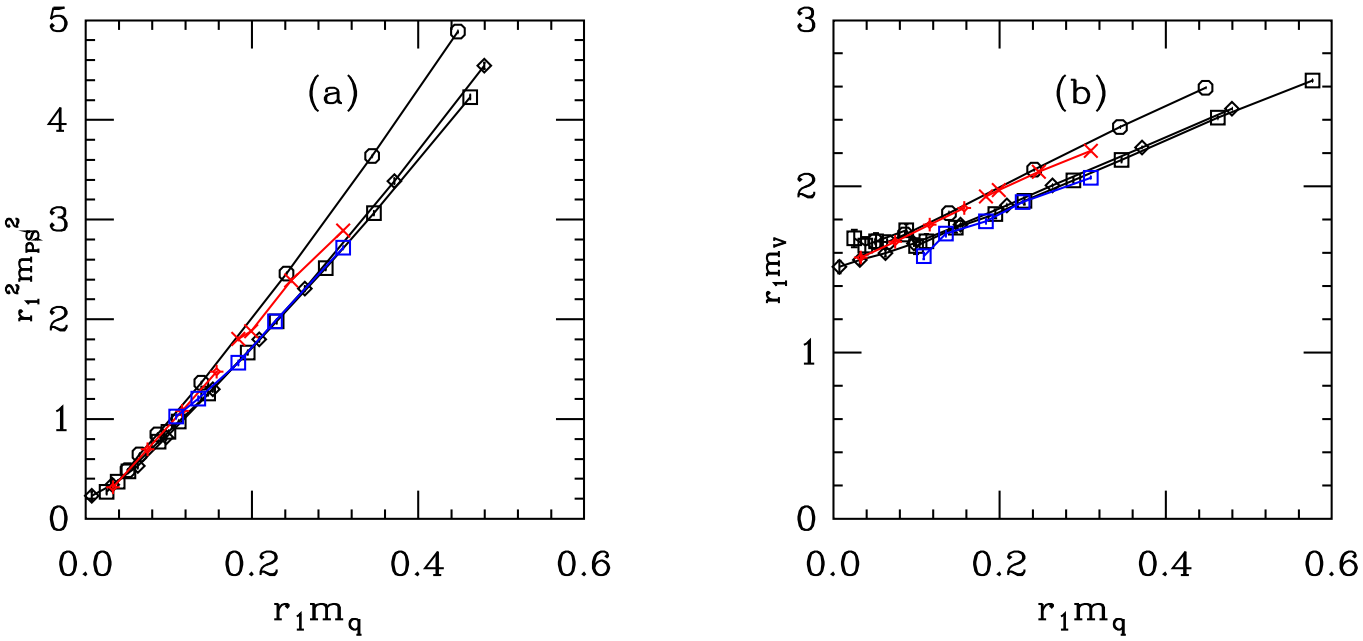

FIG. 5: Meson spectroscopy. On the left, the squared pseudoscalar mass scaled by r_1^2, on the right, r_1 times the vector meson mass. The abscissa is r_1 times the AWI quark mass. The data sets are: black squares for quenched SU(3) fundamentals, black diamonds for quenched SU(5) fundamentals, black octagons for quenched SU(7) fundamentals, red crosses for SU(4) AS2; the fancy diamonds are the PQ data. Finally, the blue squares are SU(3) with two dynamical, fundamental flavors.

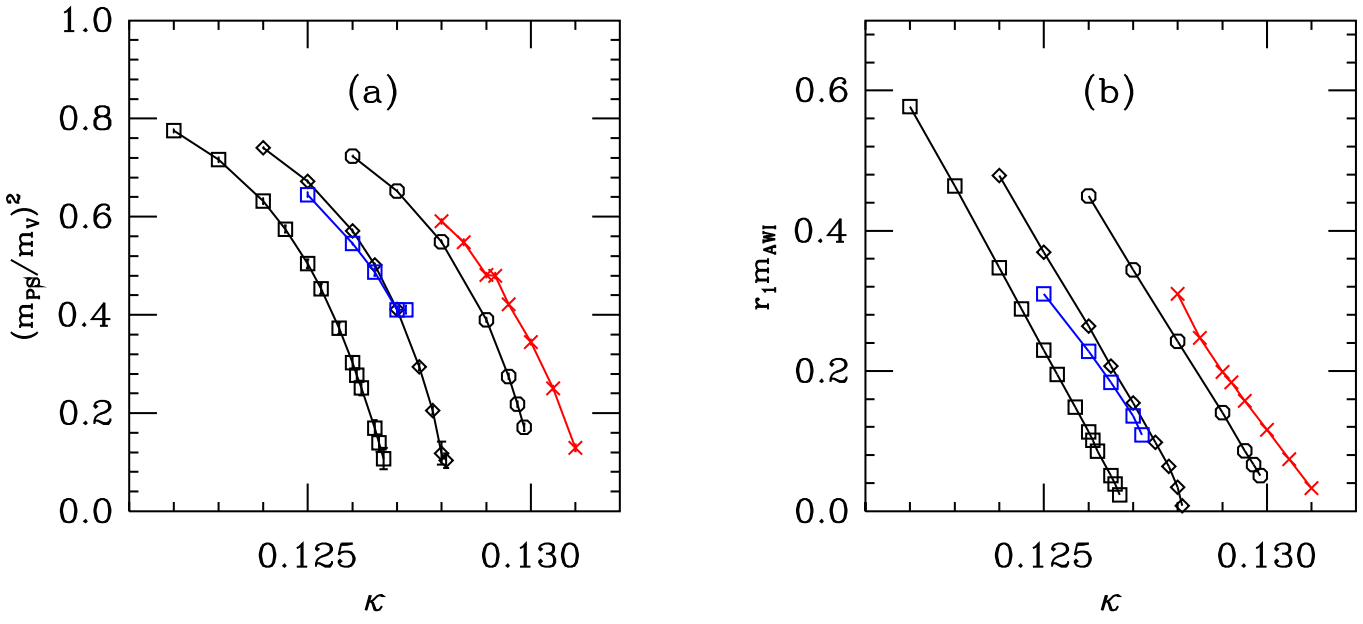

FIG. 6: Two ways to match bare parameters: panel (a) $(m_{PS}/m_V)^2$ vs κ, and panel (b) $r_1 m_{AWI}$ vs κ. The data sets are: black squares for quenched SU(3) fundamentals, black diamonds for quenched SU(5) fundamentals, black octagons for quenched SU(7) fundamentals, red crosses for SU(4) AS2. Finally, the blue squares are SU(3) with two dynamical, fundamental flavors.

κ	$aM_B(3/2)$	$aM_B(1/2)$	$a\Delta M$
0.1250	1.143(13)	1.042(7)	0.100(11)
0.1260	1.011(10)	0.926(7)	0.085(9)
0.1265	0.959(18)	0.838(11)	0.120(16)
0.1270	0.887(23)	0.748(8)	0.139(22)
0.1272	0.833(25)	0.698(8)	0.135(24)

TABLE VII: Baryon masses and splittings from dynamical SU(3) simulations. The number labels the angular momentum of the state: $M_B(1/2) = M_B(J = 1/2)$. The difference is $\Delta M \equiv M_B(3/2) - M_B(1/2)$.

AS2 theories with large N_c.

A. Spectroscopy

We plot the data for the pseudoscalar and vector meson masses in Fig. 5. To set the scale, we use the Sommer parameter r_1, and for the quark mass we use the lattice-regulated AWI quark mass, scaled by r_1 in the plots.

We display several data sets together. The new ones are the SU(4) AS2 sets, shown in red (crosses for the full dynamical sets and fancy diamonds for the partially quenched ones), and the dynamical SU(3) sets (blue squares). The black squares, diamonds, and octagons are previously published data from quenched simulations with $N_c = 3$, 5, and 7 with fundamental fermions [43].

To carry out meaningful comparisons between data obtained at different N_c's, we must match the bare parameters between the simulations in some common way. This is an inherently ambiguous procedure, but let us make the attempt. We know that hadron masses depend monotonically on the quark mass. We can compare results at the same values of the quark mass by selecting data at constant $(m_{PS}/m_V)^2$—this is a quantity which is roughly linear in the quark mass—or we can use the AWI quark mass itself, rendered dimensionless by multiplication by r_1. These comparisons are shown in Fig. 6. For both quantities, the theories can be matched over almost the entire range of κ.

We now select matching points for which we have many data sets. Thus we choose to use $(m_{PS}/m_V)^2 = 0.54$–0.56, 0.40, and 0.29–0.32 as the three ratios. We plot $r_1 m_V$ as a function of $1/N_c$, since we expect the leading corrections to scale with $1/N_c$. The result is shown in Fig. 7.

To leading order in the expansion, meson masses in both the fundamental and AS2 theories are expected to be independent of N_c [28]. Empirically, it appears that the systems connected by the original 't Hooft large-N_c scaling argument—fundamental fermions—show smaller $1/N_c$ variation than the AS2 systems over the range of N_c shown. In particular, we note that the AS2 data with $N_c = 4$ and the fundamental data with $N_c = 7$ show roughly the same shift compared to $N_c = 3$. This is seen to be the case for all quark mass values (see Fig. 5).

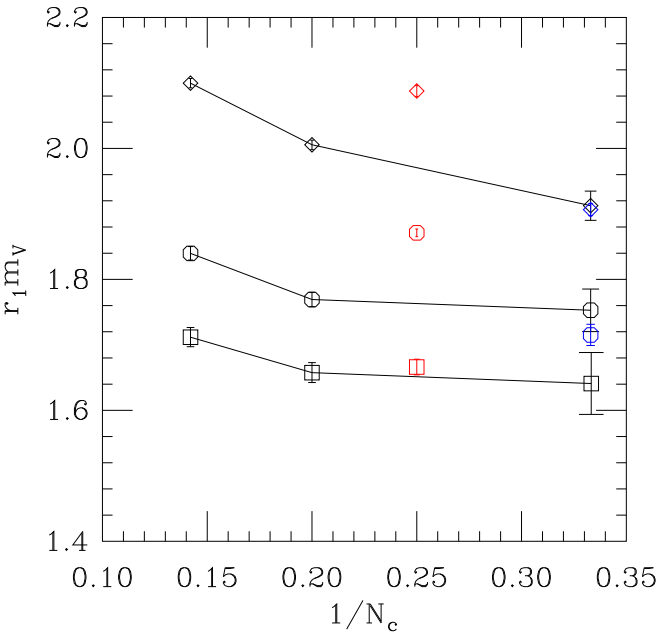

FIG. 7: Variation of $r_1 m_V$ vs $1/N_c$ for roughly matched data using $(m_{PS}/m_V)^2$. The diamonds are for $(m_{PS}/m_V)^2 = 0.54 - 0.56$, octagons for $(m_{PS}/m_V)^2 = 0.40$, and squares for $(m_{PS}/m_V)^2 = 0.29 - 0.32$. The blue symbols are the dynamical SU(3) data and the red symbols, the SU(4) AS2 data. Black symbols show quenched fundamental results.

B. Decay constants

We define the pseudoscalar decay constant f_{PS} through the matrix element

$$\langle 0|\bar{u}\gamma_0\gamma_5 d|PS\rangle = m_{PS} f_{PS} \tag{6.1}$$

(so $f_{PS} \simeq 132$ MeV), while the vector meson decay constant f_V of state V is defined as

$$\langle 0|\bar{u}\gamma_i d|V\rangle = m_V^2 f_V \epsilon_i, \tag{6.2}$$

where $\vec{\epsilon}$ is a polarization vector. With clover fermions in the usual (κ) normalization, a continuum matrix element (carrying dimension D) is defined to be

$$\langle\bar{\psi}\Gamma\psi\rangle_{\rm cont} = \left(1 - \frac{3}{4}\frac{\kappa}{\kappa_c}\right) Z_\Gamma \langle\bar{\psi}\Gamma\psi\rangle_{\rm latt} a^D, \tag{6.3}$$

and in perturbation theory for fermions in representation R the one-loop renormalization factor is

$$Z_\Gamma = 1 + \frac{g^2 C_2(R)}{16\pi^2} z_\Gamma + \cdots . \tag{6.4}$$

z_Γ for nHYP clover fermions is recorded in Ref. [67] as -1.28 for the vector current and -1.30 for the axial current. In the usual tadpole-improved analysis, one might take the coupling from the lowest-order expression for the plaquette, using the fundamental representation Casimir,

$$-{\rm Tr}\,\frac{U_P}{N_c} = g^2 \frac{C_2(F)}{4}. \tag{6.5}$$

For the quenched data sets, the plaquette values (1.787, 2.858 and 3.976) give $g^2C_2(F)$= 2–2.26. In principle, we should run the scale of the coupling from its value for the plaquette, $q^*a = 3.41$, to the values computed in Ref. [67], $q^*a \simeq 1.7$, but the combination of coupling and z_Γ is so small for nHYP fermions that, in all cases, Z_Γ is within one percent of unity.

A first determination of κ_c was described in Sec. IV. Figure 4 shows that the lattice spacing is rather strongly dependent on κ at fixed β, so one would not expect a naive extrapolation of, say, am_q or $(am_{PS})^2$ as a linear function of κ would perform particularly well. In fact, it does not; we can imagine doing fits to all four data points, or to the lightest three. Since the fits have a nonzero number of degrees of freedom, we can evaluate their quality. It is poor.

Instead, we focus on the dimensionless quantities $r_1 m_q$ and $r_1^2 m_{PS}^2$. A comparison of critical hopping parameters from the fits is shown in Fig. 8 for four possibilities, all with a linear fit:

1. From $r_1 m_q$ with all four mass values ($\chi^2 = 24.5$ with 2 degrees of freedom (dof));

2. From $r_1 m_q$ with the lowest three mass values ($\chi^2 = 2.4$ with 1 dof);

3. From $r_1^2 m_{PS}^2$ with all four mass values ($\chi^2 = 8.6$ with 2 dof);

4. From $r_1^2 m_{PS}^2$ with with the lowest three mass values ($\chi^2 = 7$ with 1 dof).

The estimates of κ_c are all quite close. More importantly, the uncertainty in the rescaling between lattice and continuum-normalized matrix elements due to different choices of κ_c is under half a per cent at any of the quark masses in our data sets. The plots below assume $\kappa_c = 0.13122$ and $Z = 1$.

The partially quenched data sets, at fixed β and sea quark κ, should all have the same lattice spacing. We should be able to find a "valence κ_c" just by fitting am_q or $(am_{PS})^2$ to a straight line. This we do, finding $\kappa_c = 0.13137$.

The dynamical SU(3) data sets have $\kappa_c = 0.12838(9)$ from a linear fit of $r_1 m_q$ in κ. The fit is stable with a χ^2 below 1.1 per degree of freedom for the lowest five masses (or fewer).

We collect our results for f_{PS} and f_V in Figs. 9 and 10. We have rescaled all fundamental-representation data by $\sqrt{3/N_c}$, and we rescaled the AS2 data by $(3/N_c)$, to remove the leading expected large-N_c scaling [25], leaving the residual. The dynamical SU(3) data sets agree with the previously-presented quenched sets (at the relatively heavy quark masses where they overlap), and the trend of remarkable N_c scaling for the fundamental-representation data contrasts with the AS2 data sets, where the shift from $N_c = 3$ to 4 is about twenty per cent.

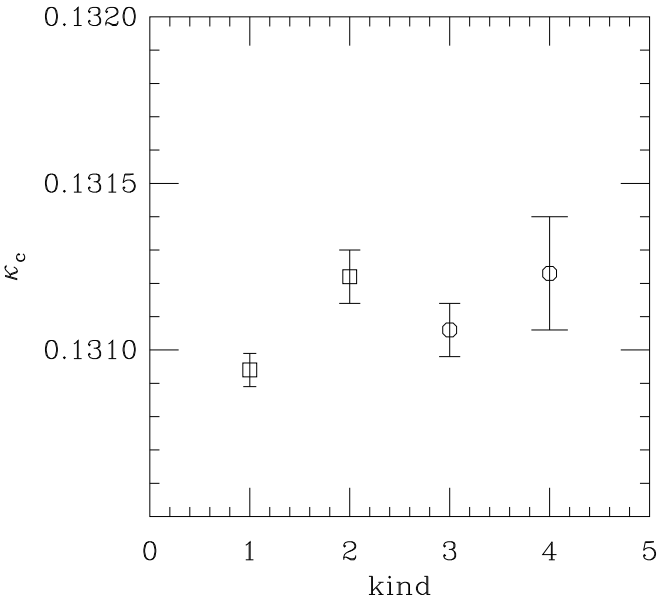

FIG. 8: Different determinations of κ_c in the SU(4) AS2 theory: (1) from $r_1 m_q$ with all four mass values; (2) from $r_1 m_q$ with the lowest three mass values; (3) from $r_1^2 m_{PS}^2$ with all four mass values; (4) from $r_1^2 m_{PS}^2$ with with the lowest three mass values.

The slope of the rescaled $r_1 f_{PS}$ with respect to $r_1 m_q$ is roughly 50% larger for the SU(4) AS2 results, compared to all other results shown. Next-to-leading order chiral perturbation theory predicts a larger contribution by a factor of 2 from the low-energy constant L_4 for the SU(4) AS2 data [68]; however, L_4 itself is usually taken to be small or even zero in QCD, since it is suppressed at large N_c (with fundamental fermions) by the OZI rule [69].[8] The OZI rule, which follows from suppression of quark loops, does not hold for the AS2 expansion [28] and so we might expect a larger slope for f_{PS} vs m_q in any AS2 theory compared to the conventional expansion at large N_c. Results at larger values of N_c with AS2 fermions would shed light on this discrepancy.

VII. COMPARISONS: BARYONS

Our baryon data are shown in Fig. 11. Unlike mesons, baryon masses depend strongly on N_c and representation. Fundamental representation data with $N_c = 3$, 5, and 7 make that point. In the figure, quenched data are shown in black while the blue points are the SU(3) dynamical-fermion data. Again, we scale the lattice masses by r_1 and plot the data versus the AWI quark mass. The

[8] Recent global analyses of the low-energy constants in QCD [70] indicate that L_4 is not necessarily small, despite the expected large-N_c suppression.

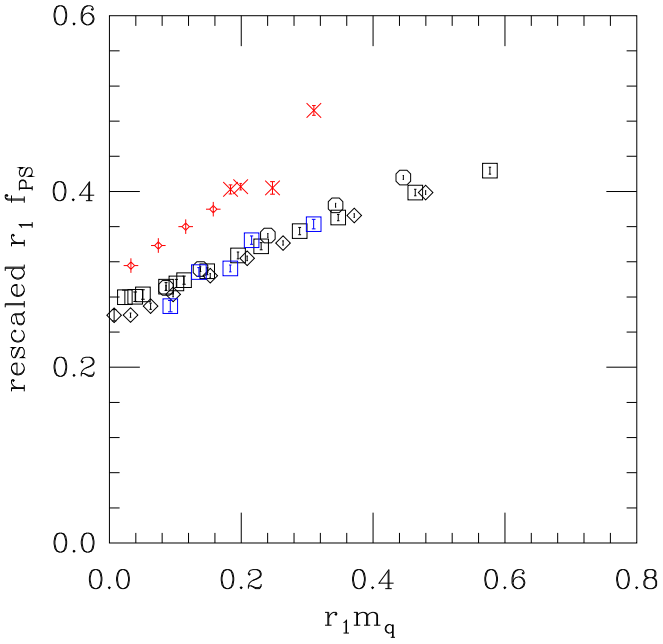

FIG. 9: Pseudoscalar decay constant. The abscissa is r_1 times the AWI quark mass. The data sets are: black squares for quenched SU(3) fundamentals, black diamonds for quenched SU(5) fundamentals, black octagons for quenched SU(7) fundamentals, red crosses for SU(4) AS2; the fancy diamonds are the PQ data. Finally, the blue squares are SU(3) with two dynamical, fundamental flavors.

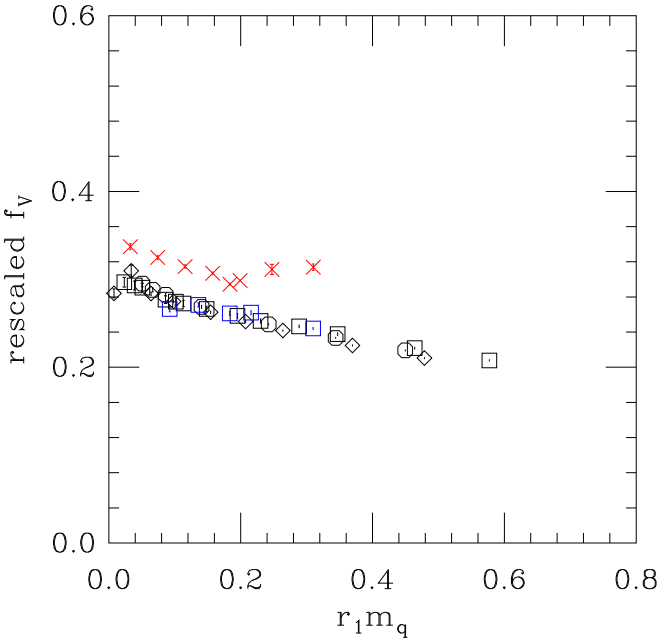

FIG. 10: Vector meson decay constant The abscissa is r_1 times the AWI quark mass. The data sets are labeled as in 9.

SU(4) AS2 masses are shown in red, with octagons for dynamical data sets and fancy diamonds for the partially quenched ones. We have used the same symbols for all states, regardless of their angular momentum, but have connected the states with the same J by lines. The masses of all the states (all N_c, all representations) are ordered in angular momentum so that higher J lies higher. Of course, the masses in each set come from the same underlying configurations, so they are highly correlated and move together as the quark mass is varied.

We can compare the fine structure in the AS2 data to the familiar rotor formula [29, 33, 37],

$$M_B(J) = m_0 N_b + B\frac{J(J+1)}{N_b}. \qquad (7.1)$$

N_b is the number of quarks in the baryon, and m_0 can be interpreted as a constituent quark mass. Thus we set $N_b = N_c$ for fundamental-representation fermions and $N_b = 6$ for SU(4) AS2. Equation (7.1) describes the data well. This is shown for one quark mass, $\kappa = 0.1285$, in Fig. 12. The masses of the four different J states are fit to two parameters, m_0 and B. The results of the fit are shown as squares in the figure. Repeating these fits for all masses, we can plot the quark mass dependence of m_0 and B. This is shown in Fig. 13.

Some residual N_c dependence is observed in Fig. 13, especially in m_0, shown in the left-hand panel. This situation for the quenched fundamental data was discussed in Ref. [44]. It was observed that the variation in the data was (noisily) consistent with a $1/N_c$ contribution to m_0; that is, $m_0(N_c) = m_{00} + m_{01}/N_c + \ldots$ where m_{00} and m_{01} were of comparable, "typical QCD" size. With only two AS2 points to compare, we cannot reliably fit for the corresponding N_c dependence. However, we observe that modeling $m_0(N_b) = m_{00} + m_{01}/N_b + \ldots$ gives roughly consistent results with our $N_c = 4$ AS2 data.

The situation for B is less clear cut: B comes from small mass differences. Certainly, the $N_c = 5$ and 7 fundamental B data and the $N_c = 4$ AS2 B data lie on a common line slightly separated from the $N_c = 3$ data. This is in qualitative agreement with large-N_c expectations, $B(N_b) = B_0 + B_1/N_b + \cdots$.

Overall, both m_0 and B are of "typical hadronic size" since $1/r_1 \sim 635$ MeV and $r_1 m_0$ and $r_1 B$ are order unity. However, they have rather different dependence on the quark mass. In the Skyrme picture, B is the inverse of the moment of inertia, scaled by N_b, so that B should be proportional to $1/m_0$. In a quark model with hyperfine interactions mediated by gluons, B is basically a product of color magnetic moments for the quarks, and for heavy quarks, the magnetic moment scales inversely with the quark mass. This suggests $B \propto 1/m_0^2$. A log-log plot of B versus $1/m_0$ certainly looks like a power law, with an exponent near unity. This is shown for $N_c = 3$ and 4 in Fig. 14 and for the quenched fundamental data in Fig. 15.

The overall dependence of the baryon mass M_B on the quark mass m_q is also interesting to study, since it may be used with the Feynman-Hellmann theorem to determine the baryonic matrix element of the scalar density, if one

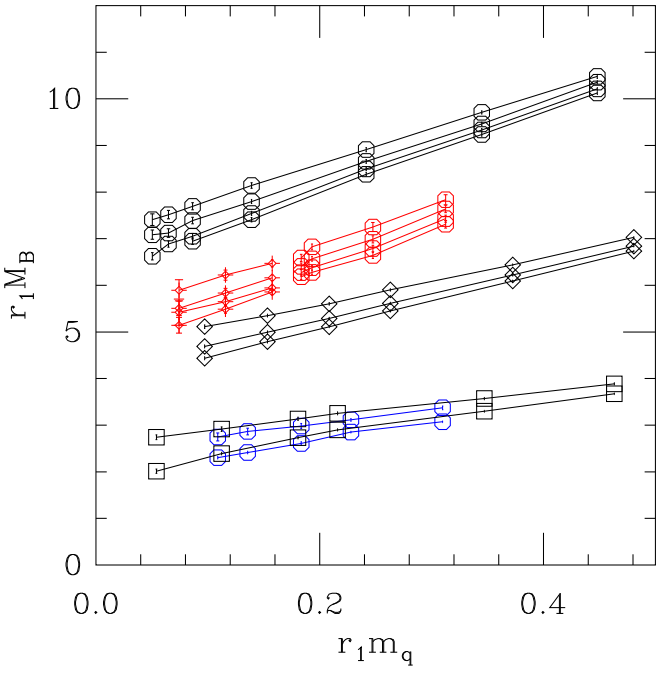

FIG. 11: Baryons. The black data are from the top quenched SU(7), SU(5) and SU(3) data. The blue octagons are SU(3) with dynamical fermions. The red points are the six-quark baryons in SU(4) AS2, octagons for dynamical and fancy diamonds for partially quenched.

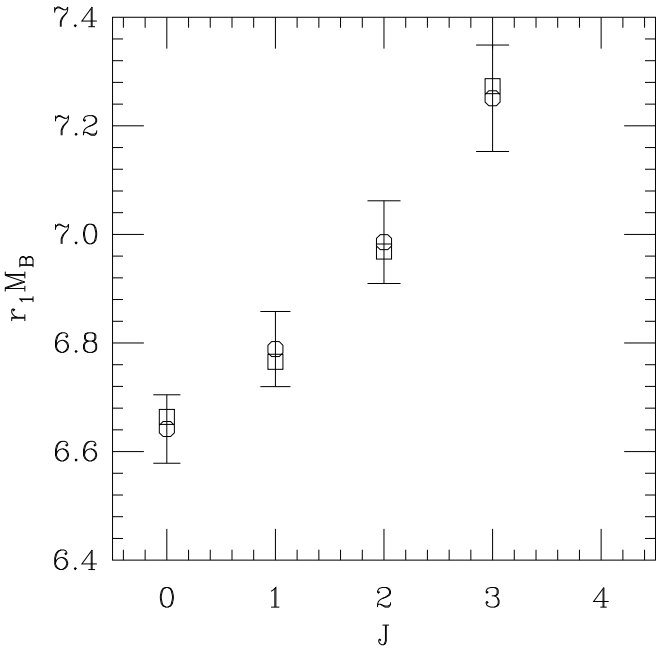

FIG. 12: Fit to rotor formula (7.1) at $\kappa = 0.1285$. Octagons (with error bars) are the data points; squares the best fit values.

defines

$$f_q^{(B)} \equiv \frac{m_q}{M_B}\frac{\partial M_B}{\partial m_q} = \frac{m_q}{M_B}\langle B|\bar{\psi}\psi|B\rangle. \qquad (7.2)$$

Multiplying by the ratio m_q/M_B cancels the renormalization of the quark mass and gives a dimensionless ratio. For the lowest-lying baryon, this quantity would determine the cross section for direct detection through Higgs exchange in the context of a composite dark matter model [46], in conjunction with the same quantity defined for matrix elements of the proton and neutron [71].

To determine the scalar matrix element, we carry out a linear fit to the quantity $r_1 M_B$ as a function of $r_1 m_q$; the resulting slope is then multiplied by m_q/M_B at each data point. To suppress possible finite-volume systematic errors, only points with $m_{PS}N_s \gtrsim 4$ are used in the fit; this excludes a small fraction of our data.

Results of this analysis are plotted in Fig. 16. Since in the limit $m_q \to \infty$ we expect $M_B \sim N_b m_q$, the quantity $f_q^{(B)}$ should approach 1 in the heavy-quark limit and 0 in the chiral limit. The functional dependence observed for all of our AS2 and fundamental data is broadly consistent at intermediate values of m_{PS}/m_V, and consistency is also seen with other lattice results for SU(2) and SU(4) theories with relatively heavy quark masses [46, 72].

VIII. CONSEQUENCES AND CONCLUSIONS

We have presented a first lattice calculation of the spectrum for an SU(4) gauge theory with two Dirac fermions in the two-index antisymmetric (AS2) representation. Because this is a real representation, its symmetries are somewhat different from the familiar QCD case; in particular the chiral symmetry group is enlarged, breaking SU(4) → SO(4). We have clarified some features of this symmetry, particularly as relevant for lattice simulations. Furthermore, we have mapped out the phase diagram for our lattice action, and identified and removed a novel discretization error in nHYP smearing which appears for real-representation fermions. Our work provides a foundation for future studies of SU(4) theories with AS2 fermions, and for other lattice studies of theories with real-representation fermions.

Comparisons of SU(4) AS2 spectroscopy and matrix elements with fundamental fermion data reveal regularities anticipated by large-N_c arguments. Although we cannot derive any quantitative results on the nature of the AS2 large-N_c expansion with only two points ($N_c = 3$ and $N_c = 4$), our results for meson and baryon masses seem consistent with the predictions of the large-N_c framework.

Scaling of decay constants seems to be less exact for AS2 fermions than for fundamental ones, with the SU(4) AS2 results clearly distinct from the various SU(N_c) fundamental theories. We note, however, that for $N_c \neq 4$,

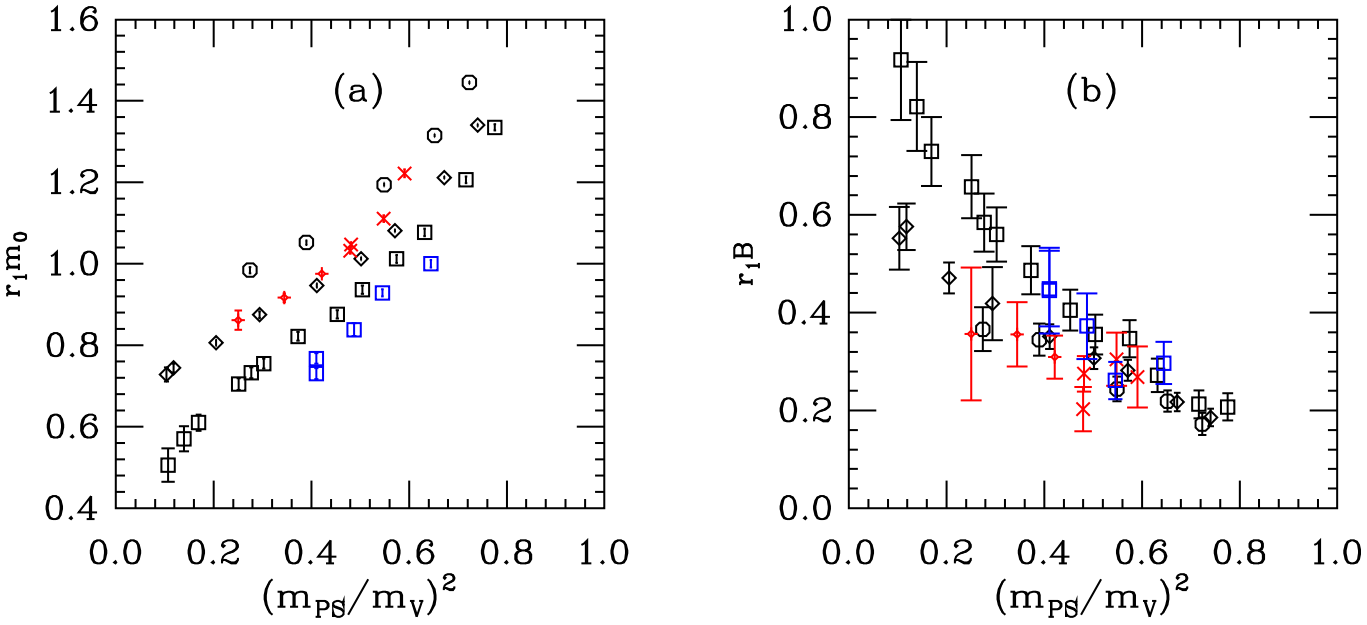

FIG. 13: The parameter m_0 (panel (a)) and B (panel (b)) from two-flavor degenerate mass data as function of $(m_{PS}/m_V)^2$ from a fit to Eq. (7.1). Data from the quenched SU(3), SU(5), and SU(7) multiplets are shown respectively as squares, diamonds, and octagons. Red crosses and fancy diamonds show the SU(4) data, unquenched and partially quenched, and the blue squares are the dynamical SU(3) data sets.

AS2 fermions live in complex representations. The pattern of chiral symmetry breaking is then identical to that of ordinary QCD. Since $N_c = 4$ is a special case, it might be an outlier for the behavior of chirally-sensitive observables such as f_{PS}.

As far as we know, no dynamical simulations of gauge plus fermionic systems on volumes large enough for spectroscopy with $N_c > 4$ have ever been performed. At heavier quark masses, however, quenching effects are not large. For future study, perhaps it would be appropriate to imagine a first round of quenched simulations with AS2 fermions. Studies of mesonic properties could be done with modest resources. With $N_b = N_c(N_c-1)/2$ quarks in a baryon, they are bosons for $N_c = 5$ (with 10 constituents), and they alternate between fermion and boson at larger N_c. Unfortunately, the number of terms in the wave function grows rapidly with N_c. Even for $N_c = 5$, the combinatorics of the lower-J correlators seem quite daunting.

Returning to the $N_c = 4$ theory, the six-quark AS2 baryons are almost certainly unstable against decay in the chiral limit, since they can fall apart into three diquarks. As an example, consider any of our baryons with $I = J > 0$. Di-quark NGBs have $I = 1$, and so the decay into 3 such NGBs is allowed by isospin conservation. However, the NGBs have $J = 0$, meaning that the baryon's angular momentum will have to be converted into an orbital motion. This leads to a kinematic suppression of the decay. The same applies to the $I = J = 0$ baryon: The isospin state of the three NGBs is antisymmetric, so they will have to be in a spatially antisymmetric state that perforce contains orbital angular momentum. Of course, knowing that the decay actually occurs as a strong-interaction process might be sufficient for phenomenology. For example, in the chiral limit of a model like this, the lightest baryon would probably not be a good dark matter candidate because it would decay into massless NGBs.

As mentioned in the introduction, of particular interest for phenomenology is the $N_{\rm Maj} = 5$ theory, whose low-energy effective theory is the SU(5)/SO(5) non-linear sigma model. We have begun a detailed study of this model that we hope to report on in the future.

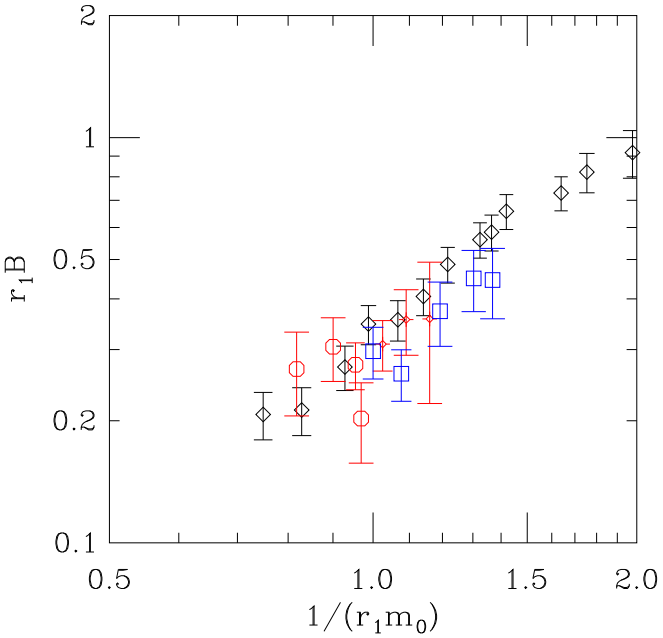

FIG. 14: B vs $1/m_0$ from the rotor formula (7.1); black diamonds from quenched SU(3), blue squares from full SU(3). The SU(4) data are shown as red octagons for the dynamical sets and fancy diamonds for the partially quenched set.

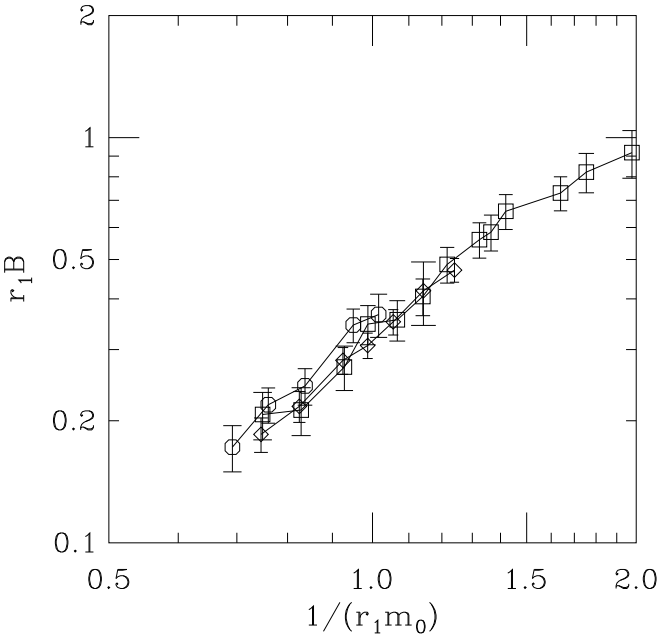

FIG. 15: For comparison, B vs $1/m_0$ from the rotor formula (7.1) from the quenched fundamental data sets of Ref. [43]: $N_c = 3$, 5, and 7 data sets are squares, diamonds and octagons.

Acknowledgments

T. D. would like to thank Richard Lebed for correspondence and conversations. B. S. thanks the University of Colorado for hospitality, as well as the Yukawa Institute for Theoretical Physics at Kyoto University. This work was supported in part by the U. S. Department of Energy, and by the Israel Science Foundation under Grant no. 449/13. Brookhaven National Laboratory is supported by the U. S. Department of Energy under contract DE-SC0012704. Computations were performed using USQCD resources at Fermilab and on the University of Colorado theory group's cluster. Our computer code is based on version 7 of the publicly available code of the MILC collaboration [73].

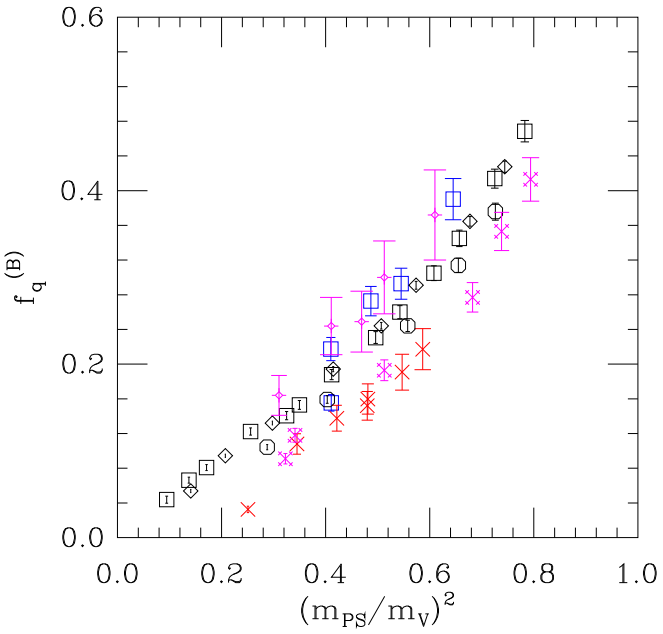

FIG. 16: The quantity $f_q^{(B)}$ defined in Eq. (7.2), plotted vs the ratio $(m_{PS}/m_V)^2$. Data shown include quenched fundamental SU(3), SU(5) and SU(7) (black squares, diamonds, octagons), dynamical SU(3) (blue squares), and dynamical SU(4) AS2 (red crosses). We also plot in purple results from [46] for quenched fundamental SU(4), for bare gauge coupling $\beta = 11.5$ (fancy diamonds) and $\beta = 12.0$ (fancy crosses).

[1] M. Perelstein, Prog. Part. Nucl. Phys. **58**, 247 (2007) [hep-ph/0512128].
[2] G. F. Giudice, C. Grojean, A. Pomarol and R. Rattazzi, JHEP **0706**, 045 (2007) [hep-ph/0703164].
[3] R. Barbieri, B. Bellazzini, V. S. Rychkov and A. Varagnolo, Phys. Rev. D **76**, 115008 (2007) [arXiv:0706.0432 [hep-ph]].
[4] R. Contino, arXiv:1005.4269 [hep-ph].
[5] B. Bellazzini, C. Csáki and J. Serra, Eur. Phys. J. C **74**, no. 5, 2766 (2014) [arXiv:1401.2457 [hep-ph]].
[6] N. Arkani-Hamed, A. G. Cohen, E. Katz and A. E. Nelson, JHEP **0207**, 034 (2002) [hep-ph/0206021].
[7] L. Vecchi, arXiv:1304.4579 [hep-ph].
[8] G. Ferretti and D. Karateev, JHEP **1403**, 077 (2014) [arXiv:1312.5330 [hep-ph]].
[9] G. Ferretti, JHEP **1406**, 142 (2014) [arXiv:1404.7137 [hep-ph]].
[10] D. B. Kaplan, Nucl. Phys. B **365**, 259 (1991).
[11] M. Golterman and Y. Shamir, arXiv:1502.00390 [hep-ph].
[12] T. DeGrand, Y. Liu, E. T. Neil, Y. Shamir and B. Svetitsky, arXiv:1412.4851 [hep-lat].
[13] E. Corrigan and P. Ramond, Phys. Lett. B **87**, 73 (1979).
[14] G. 't Hooft, Nucl. Phys. B **72**, 461 (1974).
[15] G. 't Hooft, Nucl. Phys. B **75**, 461 (1974).
[16] A. Armoni, M. Shifman and G. Veneziano, Phys. Rev. Lett. **91**, 191601 (2003) [hep-th/0307097].
[17] A. Armoni, M. Shifman and G. Veneziano, Nucl. Phys. B **667**, 170 (2003) [hep-th/0302163].
[18] A. Armoni, M. Shifman and G. Veneziano, In Shifman, M. (ed.) et al.: From fields to strings, vol. 1, 353-444 [hep-th/0403071].
[19] A. Armoni and A. Patella, JHEP **0907**, 073 (2009) [arXiv:0901.4508 [hep-th]].
[20] P. Kovtun, M. Unsal and L. G. Yaffe, JHEP **0312**, 034 (2003) [hep-th/0311098].
[21] M. Unsal, Phys. Rev. D **76**, 025015 (2007) [hep-th/0703025 [HEP-TH]].
[22] M. Hanada and N. Yamamoto, JHEP **1202**, 138 (2012) [arXiv:1103.5480 [hep-ph]].
[23] A. Cherman, T. D. Cohen and R. F. Lebed, Phys. Rev. D **86**, 016002 (2012) [arXiv:1205.1009 [hep-ph]].
[24] S. Bolognesi, Phys. Rev. D **75**, 065030 (2007) [hep-th/0605065].
[25] A. Cherman, T. D. Cohen and R. F. Lebed, Phys. Rev. D **80**, 036002 (2009) [arXiv:0906.2400 [hep-ph]].
[26] T. D. Cohen, D. L. Shafer and R. F. Lebed, Phys. Rev. D **81**, 036006 (2010) [arXiv:0912.1566 [hep-ph]].
[27] T. D. Cohen and R. F. Lebed, Phys. Rev. D **89**, no. 5, 054018 (2014) [arXiv:1401.1815 [hep-ph]].
[28] A. Cherman and T. D. Cohen, JHEP **0612**, 035 (2006) [hep-th/0607028].
[29] F. Buisseret, N. Matagne and C. Semay, Phys. Rev. D **85**, 036010 (2012) [arXiv:1112.2047 [hep-ph]].
[30] N. Matagne and F. Stancu, Rev. Mod. Phys **87**, 211 (2015) [arXiv:1406.1791 [hep-ph]].
[31] E. Witten, Nucl. Phys. **B160**, 57 (1979).
[32] E. Witten, Nucl. Phys. B **223**, 433 (1983).
[33] G. S. Adkins, C. R. Nappi and E. Witten, Nucl. Phys. B **228**, 552 (1983).
[34] J. -L. Gervais and B. Sakita, Phys. Rev. Lett. **52**, 87 (1984).
[35] J. -L. Gervais and B. Sakita, Phys. Rev. D **30**, 1795 (1984).
[36] E. E. Jenkins and R. F. Lebed, Phys. Rev. D **52**, 282 (1995) [hep-ph/9502227].
[37] E. E. Jenkins, Phys. Lett. **B315**, 441-446 (1993). [hep-ph/9307244].
[38] R. F. Dashen, E. E. Jenkins, A. V. Manohar, Phys. Rev. **D49**, 4713 (1994). [hep-ph/9310379].
[39] R. F. Dashen, E. E. Jenkins, A. V. Manohar, Phys. Rev. **D51**, 3697-3727 (1995). [hep-ph/9411234].
[40] J. Dai, R. F. Dashen, E. E. Jenkins, A. V. Manohar, Phys. Rev. **D53**, 273-282 (1996). [hep-ph/9506273].
[41] A. V. Manohar, hep-ph/9802419.
[42] E. E. Jenkins, A. V. Manohar, J. W. Negele, A. Walker-Loud, Phys. Rev. **D81**, 014502 (2010). [arXiv:0907.0529 [hep-lat]].
[43] T. DeGrand, Phys. Rev. D **86**, 034508 (2012) [arXiv:1205.0235 [hep-lat]].
[44] T. DeGrand, Phys. Rev. D **89**, 014506 (2014) [arXiv:1308.4114 [hep-lat]].
[45] A. C. Cordon, T. DeGrand and J. L. Goity, Phys. Rev. D **90**, no. 1, 014505 (2014) [arXiv:1404.2301 [hep-ph]].
[46] T. Appelquist *et al.* [Lattice Strong Dynamics (LSD) Collaboration], Phys. Rev. D **89**, 094508 (2014) [arXiv:1402.6656 [hep-lat]].
[47] M. T. Frandsen, C. Kouvaris and F. Sannino, Phys. Rev. D **74**, 117503 (2006) [hep-ph/0512153].
[48] M. I. Buchoff, A. Cherman and T. D. Cohen, Phys. Rev. D **81**, 125021 (2010) [arXiv:0910.0470 [hep-ph]].
[49] M. E. Peskin, Nucl. Phys. B **175**, 197 (1980).
[50] J. Preskill, Nucl. Phys. B **177**, 21 (1981).
[51] D. A. Kosower, Phys. Lett. B **144**, 215 (1984).
[52] R. Lewis, C. Pica and F. Sannino, Phys. Rev. D **85**, 014504 (2012) [arXiv:1109.3513 [hep-ph]].
[53] A. Hasenfratz and F. Knechtli, Phys. Rev. D **64**, 034504 (2001) [arXiv:hep-lat/0103029].
[54] A. Hasenfratz, R. Hoffmann and S. Schaefer, JHEP **0705**, 029 (2007). [hep-lat/0702028].
[55] T. DeGrand, Y. Shamir and B. Svetitsky, Phys. Rev. D **85**, 074506 (2012) [arXiv:1202.2675 [hep-lat]].
[56] Y. Shamir, B. Svetitsky and E. Yurkovsky, Phys. Rev. D **83**, 097502 (2011) [arXiv:1012.2819 [hep-lat]].
[57] S. Aoki *et al.* [JLQCD Collaboration], Phys. Rev. D **72**, 054510 (2005) [hep-lat/0409016].
[58] S. Aoki, Nucl. Phys. Proc. Suppl. **60A**, 206 (1998) [hep-lat/9707020].
[59] M. Golterman and Y. Shamir, Phys. Rev. D **89**, 054501 (2014) [arXiv:1401.0356 [hep-lat]].
[60] F. Farchioni *et al.*, Eur. Phys. J. C **39**, 421 (2005) [hep-lat/0406039].
[61] T. DeGrand, Y. Shamir and B. Svetitsky, Phys. Rev. D **82**, 054503 (2010) [arXiv:1006.0707 [hep-lat]].
[62] A. Bazavov *et al.* [Fermilab Lattice and MILC Collaborations], Phys. Rev. D **85**, 114506 (2012) [arXiv:1112.3051 [hep-lat]].
[63] D. Barkai, M. Creutz and K. J. M. Moriarty, Nucl. Phys. B **225**, 156 (1983).
[64] C. W. Bernard, T. Burch, K. Orginos, D. Toussaint, T. A. DeGrand, C. E. DeTar, S. A. Gottlieb and U. M. Heller *et al.*, Phys. Rev. D **62**, 034503 (2000) [hep-lat/0002028].

[65] R. Sommer, Nucl. Phys. B **411**, 839 (1994) [arXiv:hep-lat/9310022].
[66] A. Bazavov *et al.*, Rev. Mod. Phys. **82**, 1349 (2010) [arXiv:0903.3598 [hep-lat]].
[67] T. A. DeGrand, A. Hasenfratz and T. G. Kovacs, Phys. Rev. D **67**, 054501 (2003) [hep-lat/0211006].
[68] J. Bijnens and J. Lu, JHEP **0911**, 116 (2009) [arXiv:0910.5424 [hep-ph]].
[69] J. Gasser and H. Leutwyler, Nucl. Phys. B **250**, 465 (1985).
[70] J. Bijnens and G. Ecker, Ann. Rev. Nucl. Part. Sci. **64**, 149 (2014) [arXiv:1405.6488 [hep-ph]].
[71] P. Junnarkar and A. Walker-Loud, Phys. Rev. D **87**, no. 11, 114510 (2013) [arXiv:1301.1114 [hep-lat]].
[72] W. Detmold, M. McCullough and A. Pochinsky, Phys. Rev. D **90**, 114506 (2014) [arXiv:1406.4116 [hep-lat]].
[73] `http://www.physics.utah.edu/%7Edetar/milc/`